Fabrication and Characterisation of Ferromagnet-Superconductor bilayers

Aleena Anna Thomas

A dissertation submitted for the partial fulfilment of BS-MS dual degree in Science

Indian Institute of Science Education and Research (IISER) Mohali
April 2017

Certificate of Examination

This is to certify that the dissertation titled **Fabrication and characterisation of Ferromagnet-Superconductor bilayer systems'** submitted by **Aleena Anna Thomas** (Reg. No.MS12115) for the partial fulfilment of BS-MS dual degree programme of the Institute, has been examined by the thesis committee duly appointed by the Institute. The committee find the work done by the candidate satisfactory and recommends that the report be accepted.

Dr. Yogesh Singh Dr. Sanjeev Kumar Dr. Goutam sheet

(Supervisor)

Dated: April 20, 2017

Declaration

The work presented in this dissertation has been carried out by me under the guidance of Dr. Goutam Sheet at the Indian Institute of Science Education and Research Mohali.

This work has not been submitted in part or in full for a degree, a diploma, or a fellowship to any other university or institute. Whenever contribution of other are involved, every effort is made to indicate this clearly, with due acknowledgement of collaborative research and discussions. This thesis is a bonafide record of original work done by me and all source listed within have been detailed in the bibliography.

Aleena Anna Thomas
(candidate)

Dated: April 20, 2017

In my capacity as the supervisor of the candidates project work, I certify that the above statements by the candidate are true to the best of my knowledge.

Dr. Goutam Sheet
(Supervisor)

Acknowledgment

I would like to express my gratitude to my supervisor Dr. Goutam Sheet for his guidance and encouragement during the course of my project work. I am thankful to Dr. Sanjay Mandal, Dr. Yogesh Singh for their help. I would also like to thank my parents for their endless love and unconditional support.

I would like to acknowledge Mohammad Balal, who helped me in this project at each and every step. Furthermore I would like to thank my lab members namely Suman Kamboj, Mohammad Aslam, Leena Aggarwal, Shekar Das, Avatar Singh, Anshu Sirohi, Ritesh Kumar, Dr. Shilpa Sanwlani and Dr. Sirshendu Gayen for their help. I would like to thank my loved ones, who have supported my throughout entire process, both by keeping me harmonious and helping me putting pieces together. I will be grateful forever for your love.

List of figures

1.1 Schematic diagram of excimer (KrF) lasing action. At higher energy level, it exists as dimer and dissociate into monomer at ground state……...2

1.2 Schematic representation of pulsed laser deposition……2

1.3 Process associated with thin film deposition……5

1.4 Illustrate the motion of the electron, localisation of plasma, magnetic field loop…….....6

1.5 Schematic illustration of DC sputtering……...6

1.6 Schematic representation of physical evaporation technique……...7

1.7 Diffraction from a crystal……8

1.8 Schematic diagram of Atomic force microscopy……9

1.9 Representation of scanning electron microscopy……9

1.10 Schematic representation of vibrating scanning magnetometer. Sample is placed between pick up coils……..….10

1.11 Probe measurement of resistance temperature dependence…….10

1.12 Josephson junction in SQUID……..11

2.1 Unit cell of LSMO……..14

2.2 Double interaction between manganese atoms and oxygen through tunneled electron…15

2.3 Jahn teller distortion leads to deformation of oxygen octahedron…….16

2.4 Change in the transition temperature with respect to doping parameter……17

2.5 XRD of LSMO thin film……18

2.6 Resistance – temperature graph with a transition of 350K of LSMO thin film of thickness 30nm…….……...….19

2.7 Hysteresis loop of LSMO thin film……20

2.8 Temperature dependence of magnetization of LSMO thin film……20

2.9 Topography of LSMO thin film.……20

2.10 SEM image of LSMO pellet.....21

2.11 Elemental confirmation of LSMO thin film.……22

2.12 Topography of nickel thin film ……..…..…23

2.13 Thickness profile of Nickel thin film.……...23

2.14 MFM image of Nickel thin film.……...23

2.15 Topography of Ni/Si thin film.…….….23

3.1 Superconducting surface with limit in T_C, J_C, and H_C ……...…….25

3.2 Magnetic behaviours of type i and type ii superconductor……....27

3.3 Meissner effect of superconductor (below critical temperature) ...…….....27

3.4 Zero resistance of superconductor……..28

3.5 Structure of YBCO superconductor…….……...29

3.6 Schematic representation of YBCO thin film preparation.…….31

3.7 (a) Resistance temperature graph of YBCO thin film.……32

3.7 (b) Resistance temperature graph of YBCO pellet…….32

3.8 Non topographical image of YBCO thin film of 1.7 × 1.7 μm^2…….32

3.9 XRD of YBCO superconductor (in powder form) ...…….33

3.10 Topography of YBCO thin film of 5× 5μm^2 ……...34

3.11 XRD of BSCCO thin film.……35

3.12 R-T of BSCCO thin film.....35

3.13 Niobium thin film prepared at substrate temperature of 800°Cand power130W……37

3.14 Niobium thin film prepared at substrate temperature of 800°C and power 200W…....37

3.15 Niobium thin film prepared at substrate temperature of 800°C and power 220W…....38

3.16 Topography of Nb/Si (a) substrate temperature of 700°C……...38

3.16 (b) Nb/Si grown at substrate temperature of 600°C…….....38

3.16(c) Masked sample of Nb/Si ……39

3.16(d) Particle height distribution in Nb/Si……39

3.17 Shows the elemental analysis of Niobium thin film……39

3.18 XRD of NbN/MgO data……...40

3.19(a) Magnetic moment versus Temperature graph of Nb/STO……..…....41

3.19 (b) Moment v/s Temperature Nb/Si thin film…….……..…41

3.20 EDAX of NbN by eliminating substrate peak MgO ……..……....42

3.21 Topography of NbN/STO…….…42

3.22 Particle size distribution in NbN/STO……43

3.23 Susceptibility of TaN thin film.……44

4.1 XRD of YIG thin film on quartz……45

4.2 Topography of YIG thin film 50 × 50 μm^2in noncontact mode…….……46

4.3 MFM image of YIG thin film 35 × 35 μm^2……...46

5.1Superconductor-Ferromagnetic heterostructure thin film……...47

5.2 Vortices induced in type 2 superconductors…….……..48

5.3 Topographic image of LSMO/YBCO bilayer, with a particle size of 20nm.…….48

5.4 Hysteresis loop at 4K of LSMO/YBCO bilayer…….……49

Contents

1. General introduction

1.1 Thin film preparation technique.....1

1.2 Characterisation techniques.....7

2. Synthesis of ferromagnetic thin film

2.1 Synthesis of Lanthanum strontium manganite.....13

2.2 Synthesis of Nickel.....22

3. Synthesis of superconducting thin film

3.1 Superconductivity.....25

3.2 Synthesis of Yttrium barium copper oxide.....29

3.3 Synthesis of Bismuth strontium calcium copper oxide.....33

3.4 Synthesis of Niobium thin film.....36

3.5 Synthesis of Niobium nitride.....40

3.6 Synthesis of Tantalum nitride.....43

4. Synthesis of ferromagnetic thin film

4.1 Synthesis of Yttrium iron garnet.....45

5. Fabrication and characterisation of superconductor/ferromagnetic heterostructure

5.1 Proximity effect in superconductor/ferromagnetic heterostructure.....47

5.2 LSMO-YBCO heterostructure.....48

5.3 Conclusion.....49

Abstract

We are looking at magnetic pinning of vortices induced in Superconductor-Ferromagnet heterostructure. We prepared thin films of YBCO, LSMO, BSCCO, Nb , NbN, TaN through pulsed laser deposition and magnetron sputtering. The stoichiometry of thin film were characterized by XRD and EDAX, Surface morphology, grain size and the thickness measurements have been done by Atomic Force Microscopy and for superconducting and ferromagnetic properties we performed electrical and magnetic transport measurements viz. ac susceptibility, four-probe resistivity and VSM. We are also investigating vortices using low temperature magnetic force microscopy.

Chapter 1

General Introduction

1.1 Thin film preparation technique

A thin film can be defined as a quasi two dimensional material created by condensing, atomic/molecular/ionic species of matter. Thin film technology is well established and is the demand of twenty first century, for the development of new materials. There are several techniques available for thin film preparation depending upon the desired film and substrate. The most important thin film preparation methods are DC-sputtering, RF sputtering, pulsed laser deposition, Thermal evaporation [6].

1.1.1 Pulsed laser deposition

Pulsed laser deposition is a research tool for the synthesis of variety of thin film. A target of polycrystalline material is locally heated by focussed laser pulse leading to instantaneous heating and evaporation of target material. The evaporated material is further heated by the high-pressure plasma of ionised target atoms. The plasma expands from the target and directed towards the substrate due to high pressure gradient. Finally plasma reaches to substrate and gets deposited on it. The shape of the plasma plume leads to an even distribution over the surface. After reaching the substrate, the target atom uses their remaining kinetic energy to diffuse over the surface. The kinetic energy of the atoms reaching the substrate can be influenced by the process parameter. The frequency and energy density of the laser which determines the amount of the material ejected out and its energy. High quality thin film which is uniformly deposited can be achieved through optimising various processing parameters [1].

KrF laser is an excimer (UV region) laser with pulse duration of 10 to 50 ns and a wavelength of 248nm.

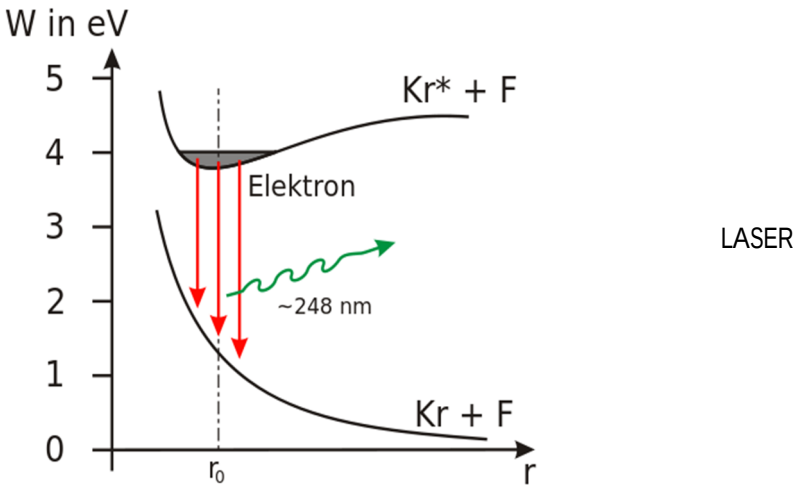

Figure1.1: Schematic diagram of excimer (KrF) lasing action. At higher energy level it exists as dimer and dissociate into monomers at ground state.

(Source: http://www.wikiwand.com/de/Excimerlaser)

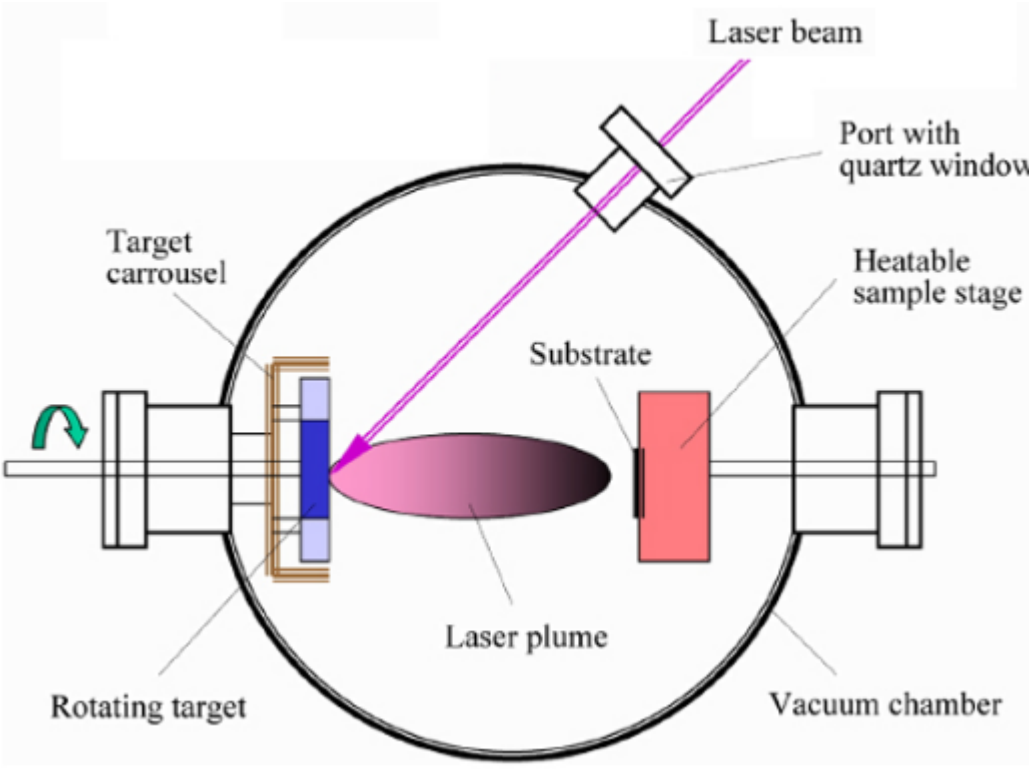

Figure 1.2: Schematic representation of PLD (source: http://titan.physx.u-szeged.hu/~lamilab/plden.htm)

1.1.2 Mechanism of PLD process

Pulsed laser deposition is a complex process. Solid surface is exposed to intense laser beam; a small amount of target material from the surface is vaporized and ejected from the sample. The vapour consists of collection of atoms, ions, molecules etc. And kinetic energy of these species depends on the laser parameter (intensity, pulse width). Atlas, vapour comes in contact with the surface and re-condenses on to the surface. The quality of a thin film is determined by many parameters such as choosing ideal substrate, substrate temperature, background pressure, rate of deposition of material by the plume, laser intensity, laser pulse duration, choice of wavelength for excitation and background gas[2][3].

Laser process can be confine to following steps:

1. Laser –target interaction
2. Plume expansion
3. Film deposition

1.1.3 Laser –target interaction

The evaporation of material from the surface of target material depends on laser target interaction. The intense heating of material by nano-pulsed laser is followed by melting and evaporation of surface layers in depth. The thermal parameter of heating, melting depends on laser parameter (laser duration, energy, intensity), material properties (heat capacities, reflectivity, absorption coefficient, thermal conductivity.

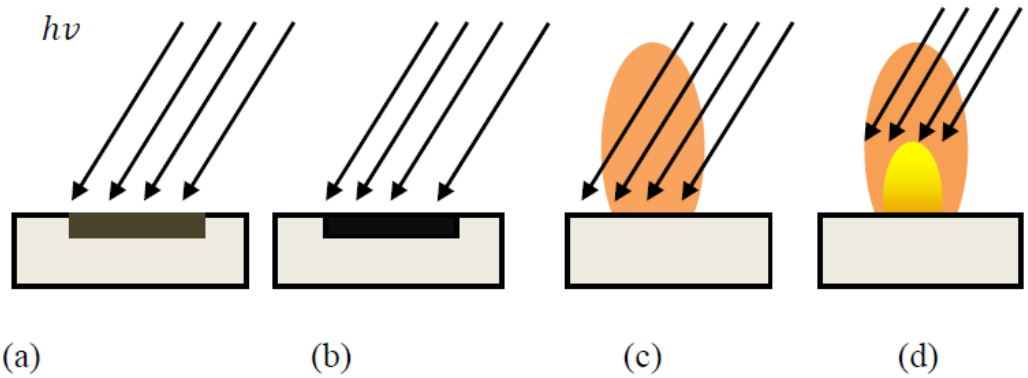

(a) Laser hit the target surface

(b) It melts the target surface

(c) Plasma is forming

(d) Target material dislodged into the plasma.

1.1.4 Plume expansion

Plume expands freely and adiabatically in vacuum inside the PLD chamber. Plasma formed is perpendicular to the surface of the target. The colour of the plasma is due to the collision between the particles in it. During the plasma expansion, internal thermal and ionization energies are converted into kinetic energy of the ablated species. When plasma expands temperature decreases. The expansion of plume highly depends on the background gas, which is non- reactive.

1.2.4 Thin film deposition

Material which is ablated hits the substrate. Target particle collide with substrate and condense them on the surface. The factors affecting the film growth are density, energy, condensing material, substrate etc. The surface morphology of a thin film is determined by nucleation and growth process. Nucleation leads to condensation of material from vapour to solid phase. When supersaturated gas phase is reached, nucleation starts.

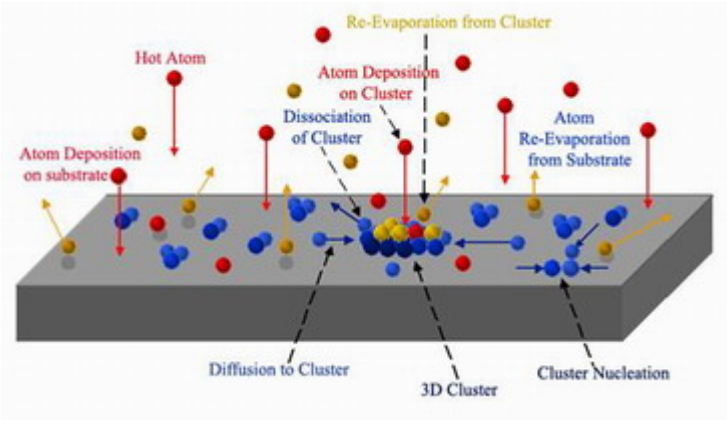

Figure 1.3: Processes associated with thin film deposition.

(Source: http://academic.uprm.edu/pcaceres/Research/Combi/id3.htm)

1.1.2Magnetron sputtering

Magnetron sputtering is plasma vapour deposition process in which plasma dislodges the ablated material to the substrate. We are applying a negative potential on to the target in high vacuum. Positively charged ions gets accelerated towards the target and dislodge atoms from target. Conductive materials are deposited by using DC power supply and insulators by radio frequency. In magnetron sputtering there is a closed loop of magnetic field to trap the electrons. This field enhances the efficiency of initial ionisation and generation of plasma.

Magnetron is made up in different geometries. The basic underlying principle of magnetron sputtering is to trap plasma in between the magnetic and electric field. The range of magnetic field will depend upon the geometry of the magnetron.

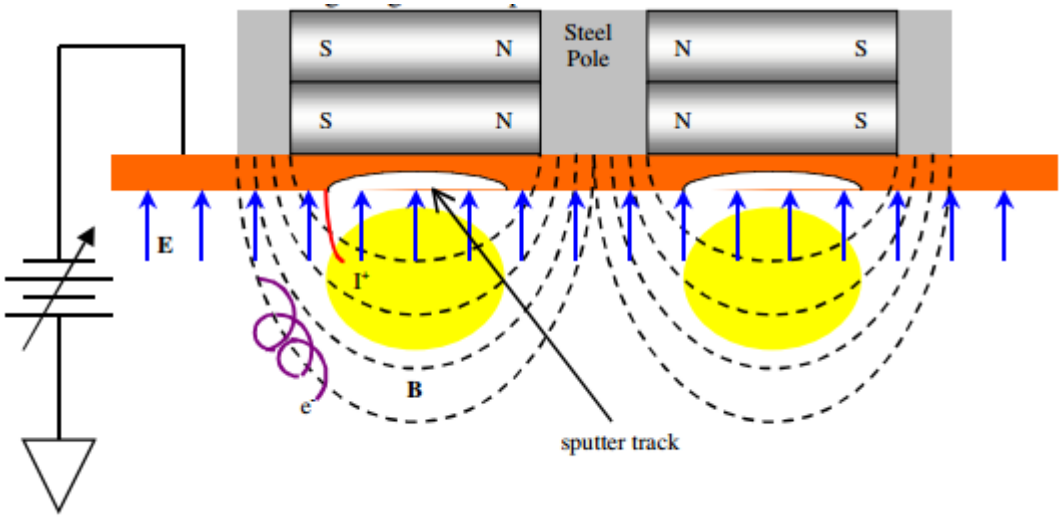

Figure 1.4: Illustrates the motion of the electron, localisation of plasma, magnetic field loop.
(Source:https://askubuntu.com/questions/707900/invert-colors-change-to-grayscale-as-a-toogle.)

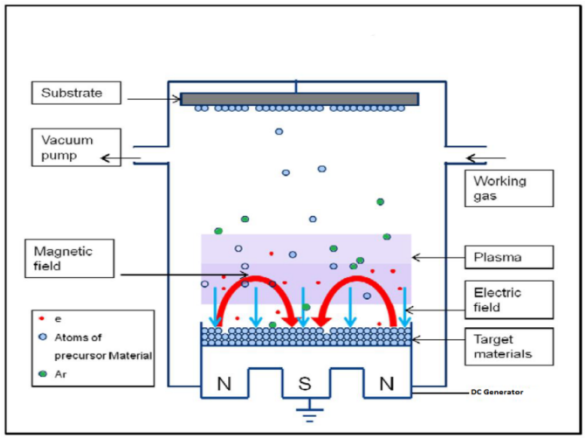

Figure 1.5: Schematic illustration of DC sputtering process.
(Source:https://www.slideshare.net/ewqasdfghjkl/sputtering-51343247)

Physical vapour deposition

In physical vapour deposition the depositing material is directly converted to vapour phase. For evaporation we heated the crucible by introducing energy in the form of current to raise the temperature. Evaporation is based on the concept that there exists a vapour pressure for any material at which it sublimes. One of the greatest advantages is that highest purity due to low pressure. PVD is highly versatile technique that enables to deposit all type of inorganic materials.

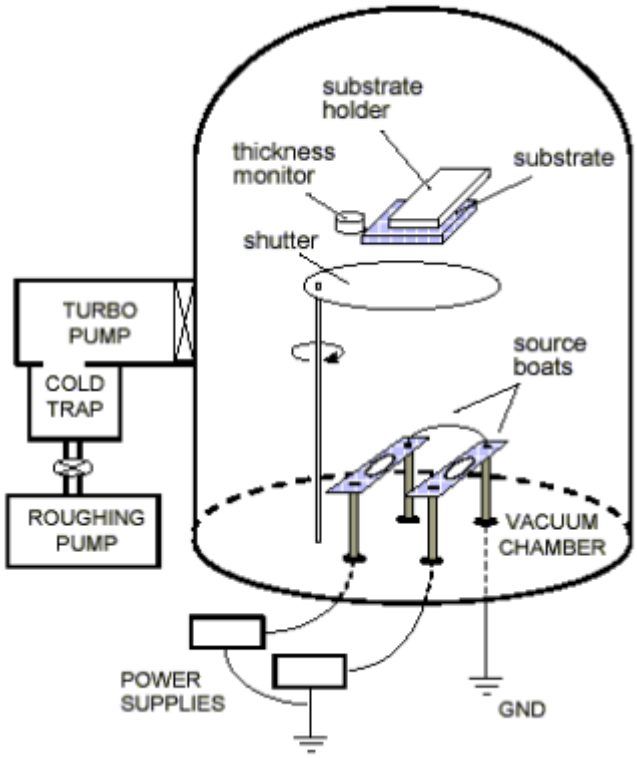

Figure 1.6: Schematic representation of physical evaporation.

(Source:https://stuff.mit.edu/afs/athena.mit.edu/course/3/3.082/www/team2_f02/Pages/processing.html).

1.2 Characterisation techniques

1.2.1 X-ray crystallography

X-ray crystallography helps up to understand the molecular and crystal structure. Atoms are arranged in a periodic fashion to form lattice in a crystal, it will undergo interference to give rise to the maximum intensity peak. This is governed by the Bragg's law.

$$n\lambda = 2d \sin\theta$$

Where n is the order of the diffraction, λ is the wavelength, d is the inter-planar distance, θ angle of diffraction.

A narrow beam of X-ray coming X-ray source (synchrotron, x-ray tubes) is allowed to fall on the sample at an angle θ and a detector is placed at 2θ with respect to incident radiation. During the measurement the source is fixed but sample and detector are

allowed to rotate. The intensity of the peak implies the stoichiometry and quality of the texture of the sample.

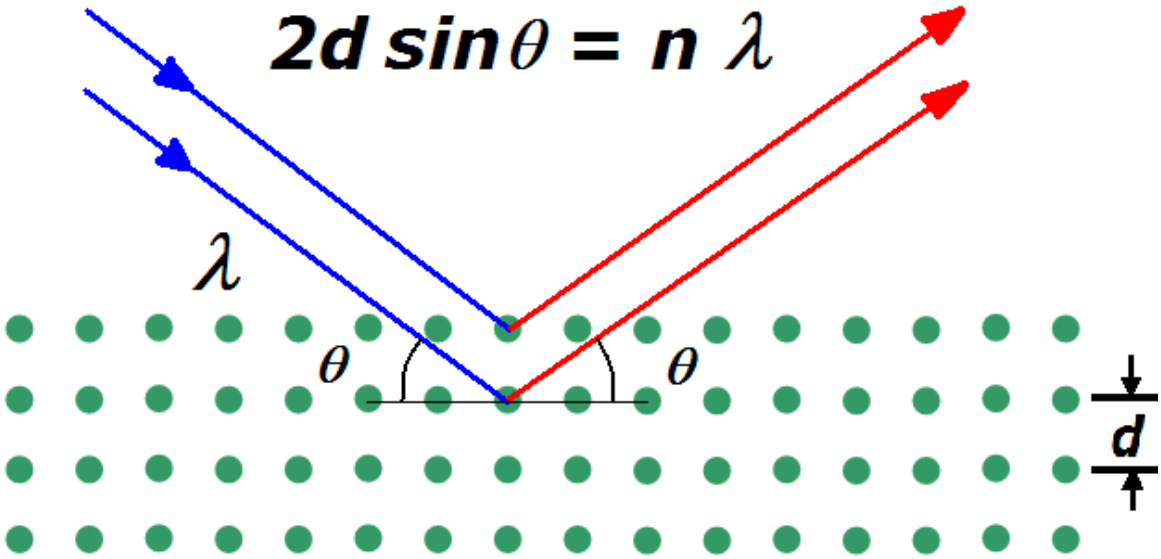

Figure 1.7: Diffraction from a crystal

1.2.2 Atomic Force Microscopy

Atomic force microscopy (AFM) is a scanning probe microscopy which has a tip atomically touches the sample. Tip is allowed to move back and forth so it can measure topology with atomic resolution. We can do AFM in room temperature. AFM can be done in different mode one is contact mode and the other is non contact mode. In contact mode tip will touches the sample whereas in non contact mode tip will be at a distance of few nanometres. Reflected laser beam from cantilever is detected by position sensitive cantilever [4] [5].

For investigating magnetic domains in the system AFM system, we use Magnetic Force Microscopy (MFM) mode. In this case we keep tip at a distance of 50-100 nm so that tip will be get rid from all other forces such as Vanderwaals and experience only magnetic interaction. MFM helps to manipulate the magnetic interaction between the sample and the tip. Thus we can manipulate the magnetic domains in a material.

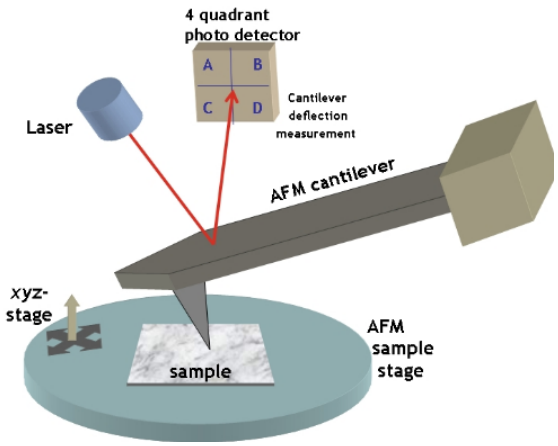

Figure 1.8: Schematic diagram of AFM. (Source: https://simple.wikipedia.org/wiki/Atomic_force_microscope).

1.2.3 Scanning electron microscopy

Scanning electron microscopy gives the information about external morphology. In SEM electron beam will act as source. It will give an idea about surface morphology and grain size of the particle. It has additional facility named as EDAX for elemental analysis.

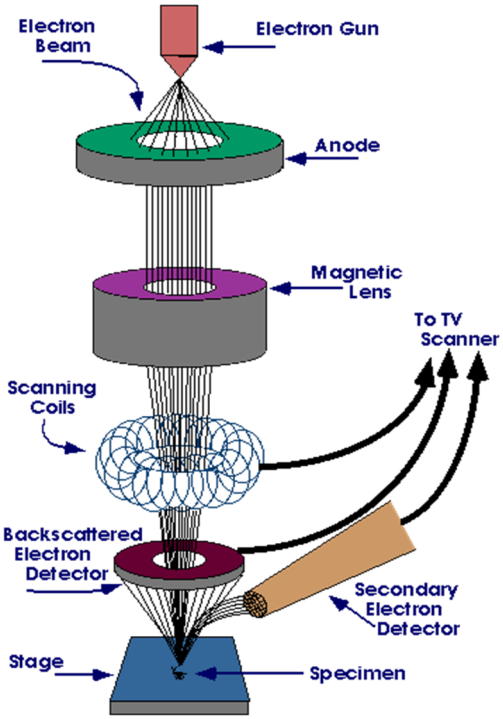

Figure 1.9: Schematic representation of SEM.
(Source:http://www.crestdit.com/Services/SEM.html)

1.2.4 Vibrating Sample Magnetometer (VSM)

VSM is an important technique to measure magnetic moment. In VSM system sample (which shows magnetic behaviour) is kept between two pick up coil. The vibrating sample was kept at the centre of coils which results in the change of flux through the coil there by change in the induced voltage. The voltage induced is directly proportional to the magnetic moment of the sample.

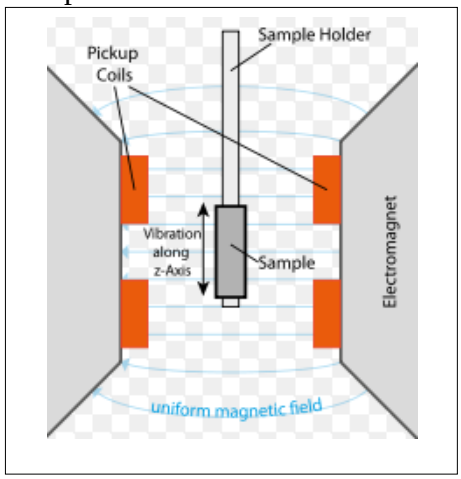

Figure 1.10: Schematic representation of VSM. Sample is placed between pickup coils.

(Source: http://nptel.ac.in/courses/115103030/30)

1.2.5 Low Temperature Resistance Temperature System

Low temperature dependence of resistance was measured using four probe method. We are making four contacts on the surface of the sample using gold wire and silver paint. Sample is kept in R-T probe which scan the temperature from 2K to 300K. We are passing current through two contact and measuring voltage by using other two contacts.

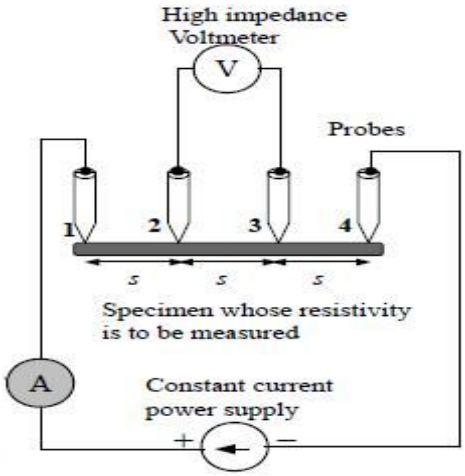

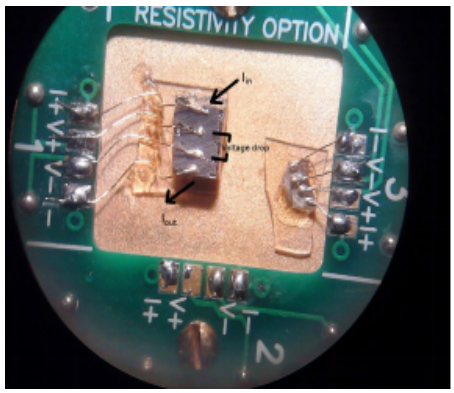

Figure 1.11: Four probe measurement for resistance – temperature dependence

1.2.6 Superconducting Quantum Interference Device Magnetometer (SQUID)

SQUID uses the Josephson Effect to measure the change in magnetic flux. SQUID comprises of two superconductors separated by thin insulating layer. SQUID is able to detect even small magnetic field. If a constant current is maintained in SQUID device then voltage measured will change depending upon phase change across the junction this will result in change in magnetic flux. Two superconductor separated by an insulator can tunnel cooper pair of electron through the junction. Cooper pair on each side of the junction can be represented by the wave function of free particle. In DC Josephson junction, current is proportional to phase difference of wave function across the junction in the absence of voltage. While in AC Josephson junction oscillate in a characteristic frequency is proportional to the voltage across the junction. Since Josephson junction can measure the frequency with great accuracy so it is considered as the standard measure of voltage.

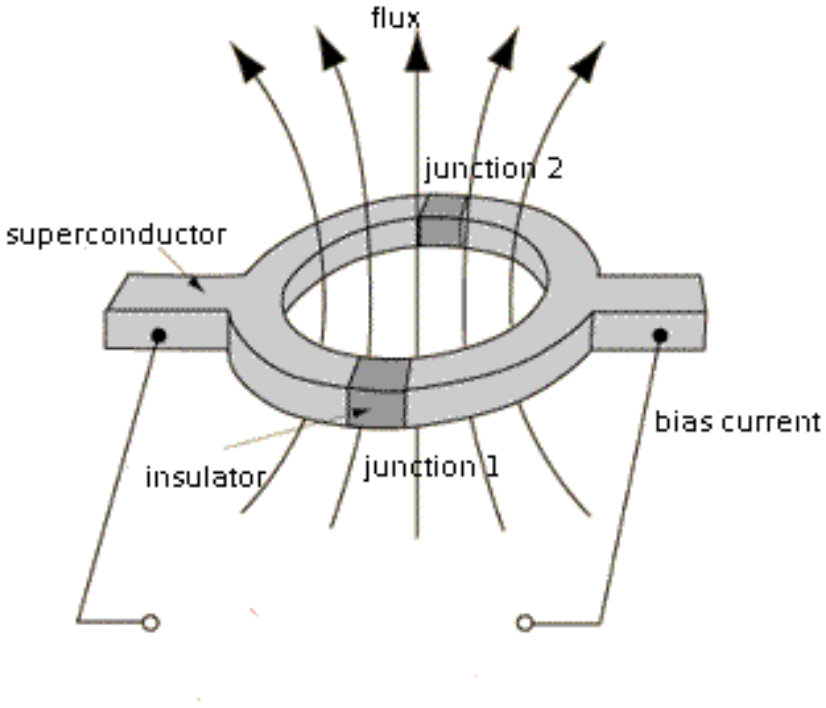

Figure 1.12: Josephson junction in SQUID.

(Source: http://hyperphysics.phy-astr.gsu.edu/hbase/Solids/Squid.html).

Chapter 2

Synthesis of Ferromagnetic thin film

The existence of magnetic field even in zero applied fields is the characteristic feature of a ferromagnetic material. Existence of spontaneous magnetic moment implies that the electron spin and magnetic moment aligned in one direction.

B_E is considered as magnitude of exchange field. In the mean field approximation, we assume each magnetic atom experiences a field proportional to the magnetization.

$$\boldsymbol{B_E = \lambda M}$$

Magnetisation (**M**) is defined as magnetic moment per unit volume. Where λ is constant, which is independent of temperature.

The Curie temperature T_C is the temperature above which spontaneous magnetisation disappears. When $\boldsymbol{T > T_c}$ it is in a disordered state become ordered state at$\boldsymbol{T > T_c}$.

In an applied field, $\boldsymbol{B_a}$ will cause a finite magnetization and in turn a finite exchange field $\boldsymbol{B_E}$. If $\boldsymbol{\chi_P}$is the paramagnetic susceptibility

$$\boldsymbol{\mu_0 M = \chi_P (B_a + B_E)}$$

Curie's law is given by $\boldsymbol{\chi_P = {C}/{T}}$

Where, C is Curie constant.

$$\boldsymbol{\chi = {M}/{B_a} = {C}/{(T - T_C)}}$$

If χ is infinite we can have a finite M for zero $\boldsymbol{B_a}$. We have Curie–Weiss law.

$$\boldsymbol{\chi = {C}/{(T - T_C)}}$$

2.1 Synthesis of Lanthanum Strontium Manganite ($La_{0.7}Sr_{0.3}MnO_3$)

LSMO is a ferromagnetic which has potential application in spintronics because of high Curie temperature (T_C-370K) and its half-metallic nature [8]. Lanthanum strontium manganite (LSMO) is an oxide with perovskite crystal structure. The chemical composition of LSMO is $La_{1-x}Sr_xMnO_3$, where x denote doping factor. Perovskite is a crystal structure in which manganese atom is surrounded by the octahedron of oxygen atom. The lanthanum is in +3 oxidation state, oxygen in -2, and manganese can be in +3 or +4 oxidation state. The electrical and magnetic behaviour of LSMO is determined by the number of electron present in the d shell of manganese atom. Doped perovskite manganites exhibit unique electronic, magnetic and transport properties such as colossal magneto resistance, spin polarisation, large resistance change at metal insulator transition, double exchange interaction etc.

The reason behind the electrical and magnetic properties is based on interaction between manganese atoms. The interaction is of different types such as double exchange interaction, super exchange interaction, Jahn teller effect and charge ordering.

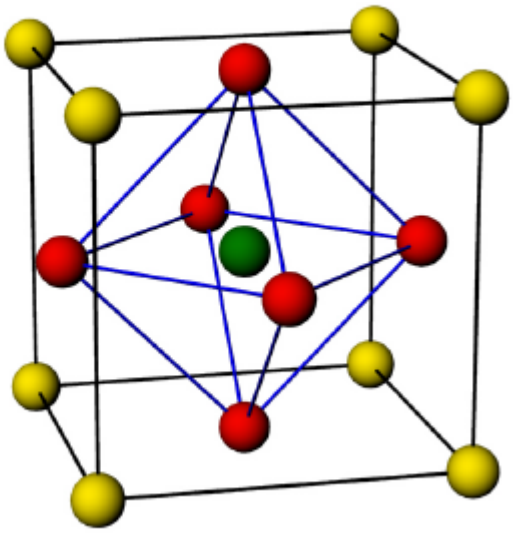

Figure 2.1: Unit cell of LSMO

Lanthanum (La^{+2})/ Strontium (Sr^{+2}) yellow coloured

Oxygen is surrounded octahedral (O^{2-}) red coloured

Manganese ($Mn^{+3/+4}$) green coloured

2.1.1 Double interaction

Double exchange interaction is a process in which two neighbouring manganese atom and the connecting oxygen atom play a major role. The process can be explained using illustration in the Figure2.2. One of the manganese atoms having its one electron in e_g state, and the other manganese atom with empty e_g state. One electron from the oxygen gets tunnelled to the manganese atom without e_g electron. The e_g electron from the other manganese atom will tunnel to the freed 2P position of oxygen. The net movement of electron from one manganese to other manganese via oxygen is defined as double interaction which leads to electrical conductivity. Tunnelling can take place between states having parallel spins. Double interaction can only occur to increase the freedom of electrons, it lowers their energy. This makes it energetically favourable for electrons of neighbouring manganese atoms to align their spins, inducing ferromagnetism. Double interaction depends on the filled and empty e_g states which is highly doping dependent.

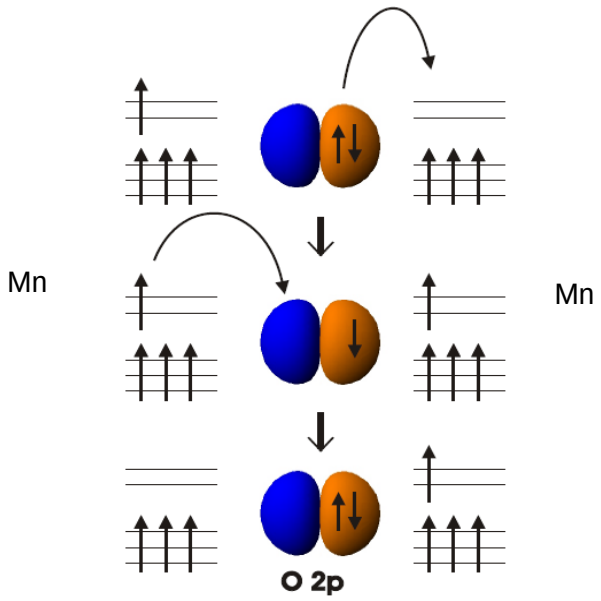

Figure 2.2: Double Interaction between manganese atoms and oxygen atom through tunnelled electron

2.1.2 Jahn teller effect

The Jahn teller effect is an interaction between the crystal lattice and the manganese 3d electrons [8]. There arise an energy difference in degenerate t_{2g} and e_g state due to the deformation of oxygen octahedron as shown in the Figure 2.3. When the e_g crystal is half

filled it is energetically favourable to create a deformation because one of the orbital will lose energy. The electron in the e_g shell will occupy this lower energy state, creating a deformation of the oxygen octahedron without altering the overall crystal lattice leads to typical Jahn teller distortion as shown in the Figure 2.3.

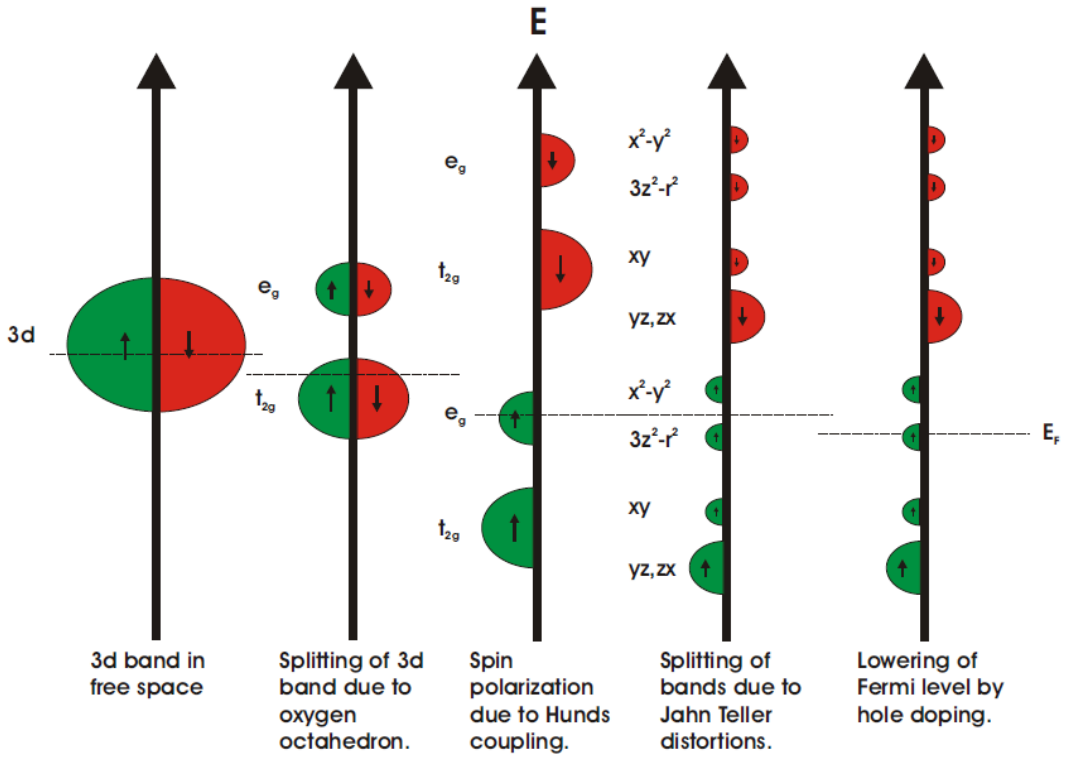

Figure 2.3: Jahn teller distortion lead to deformation of oxygen octahedron

2.1.3 Charge ordering

Charge ordering is because of columbic repulsion between different manganese atoms. The electron formats a pattern by them to reform the lattice. The configuration of electron is so stable that each electron will retain its position. Two reasons are attributing to their stability. One is columbic repulsion and the second one is because of electron phonon coupling where electron locally deforms oxygen octahedron.

2.1.4 Phase diagram

The above mentioned factors are responsible for the electrical and magnetic characteristic of LSMO. The temperature, sample doping, strain etc will determine which mechanism is

predominant. The phase diagram (Figure 2.5) clearly indicates the behaviour of LSMO. LSMO is ferromagnetic and have high Curie temperature of 370K.

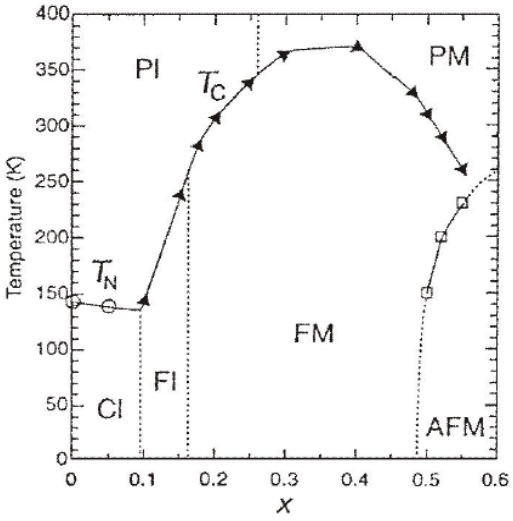

Figure 2.4: The change in the transition temperature with respect to doping parameter (x)

Synthesis and Fabrication

2.1.5 LSMO target preparation

In this study, we want to prepare LSMO target for pulsed laser deposition. Target was prepared by mixing of La_2O_3, $SrCO_3$, and MnO_2 in the correct proportion.

$$La_2O_3 + SrCO_3 + MnO_2 \rightarrow La_{0.7}Sr_{0.3}MnO_3 + CO_2$$

The precursor powder mixture was intimately mixed by grinding agate mortar for 3-4 hours to get black powder of LSMO. Grounded sample was taken in an alumina crucible and subjected to calcinations at 920°C for 6 hours. Muffle furnace was used for calcinations and sintering. During calcinations there is a change in phase of sample take place. The actual solid state reactions take place during calcinations, where reaction between the constituents resulting to a desired phase of material. The right temperature and the rate of cooling will determine electrical and mechanical properties of the material. Whereas during sintering densification of the material take place. After calcinations black powder was regrind and made a big pellet using hydraulic press and kept for sintering at 1200°C for 20 hours. Polycrystalline sample was characterised by X-ray crystallography.

2.16 Thin film preparation of LSMO using pulsed laser deposition

LSMO thin films were grown on oxygen annealed single crystal substrate of strontium titanate $SrTiO_3$ (100) using pulsed laser deposition (PLD) [8]. Depositing a stoichiometric target (LSMO pellet) in an oxygen pressure of 0.31mbar having a background pressure10^{-6} mbar. The substrate temperature was at 800°Cfor one hour and base pressure was 10^{-6} mbar. KrF excimer laser operating at 248nm with energy of 235mJ, laser frequency of 4Hz and 12000 shots is used.

2.17 Characterisation techniques

Structural analysis -X-ray Crystallography

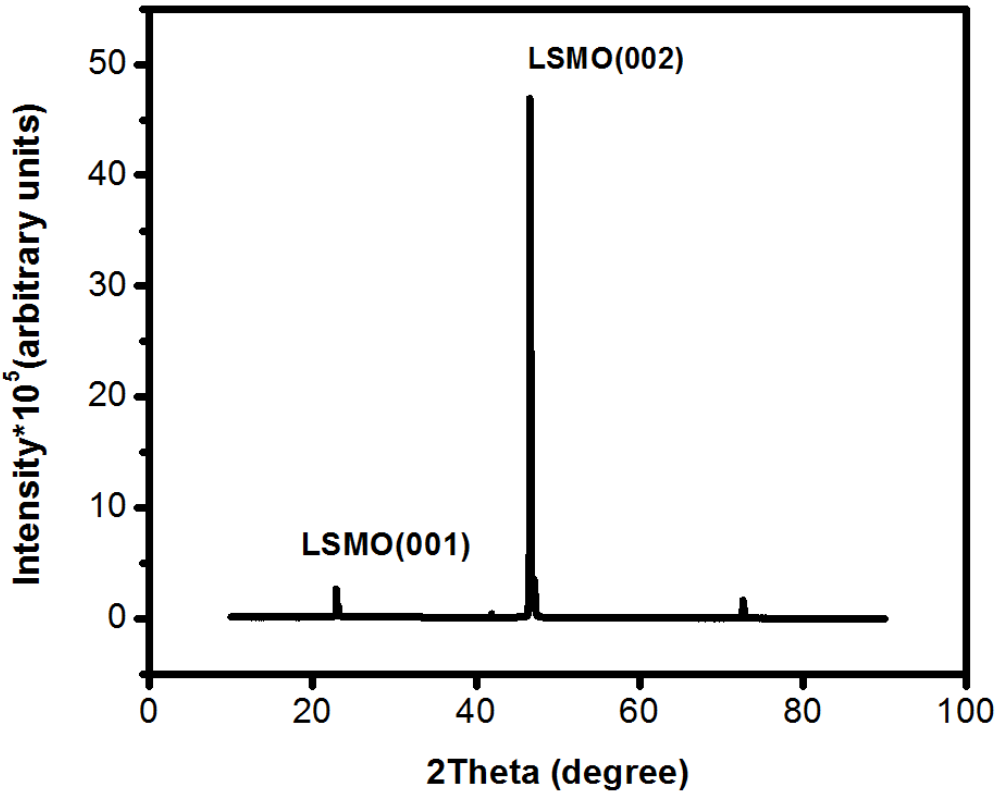

Figure 2.5: XRD of LSMO thin film

From the Figure 2.5 gives the θ-2θ XRD patterns of LSMO films on STO substrate. From the graph it implies that LSMO film is highly c-axis oriented and has lattice constant of 3.855 A^0 for STO substrate (lattice parameter-3.905 A^0). It is confirmed the stoichiometry of LSMO thin film is $La_{0.7}Sr_{0.3}MnO_3$.The experimental out of plane lattice parameter c value from (001) (23.54), (002) (43.34) respectively.

Resistance – Temperature measurement (Four Probe)

Resistance temperature graph indicates the metal insulator transition temperature. When temperature increases resistances also increases which is a metallic behaviour. The graph is showing metallic behaviour till the transition temperature and afterward it has insulator characteristics. The transition is broad and shows a drastic change in resistance. Transition temperature is 350K, which is an indication for its doping factor.

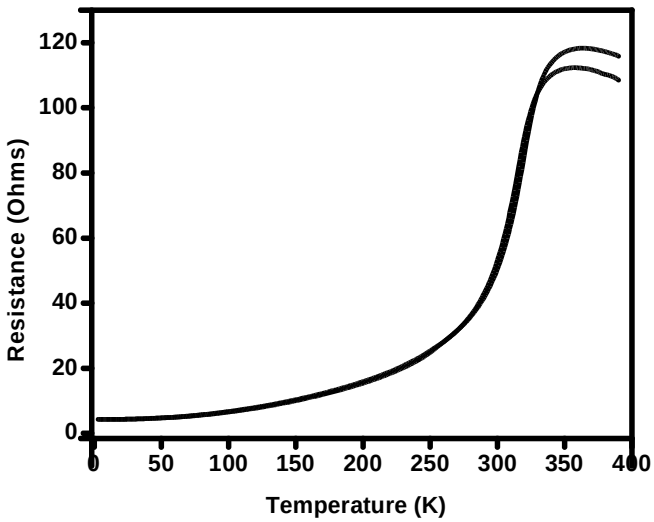

Figure 26: Resistance –temperature graph with a transition of 350K of LSMO thin film of thickness 30nm and zero magnetic fields.

Magnetic properties

Graph 2.7 (a) is magnetic moment (M) versus magnetisation (H) and 2.7 (b) image of hysteresis loop (zoomed version of first graph).Magnetic moment exist even at after the removal of external magnetic field. This is called retentivity. The amount of reverse magnetic field should be applied to make the net magnetic moment zero is the coercivity of magnetic material.

(a) (b)

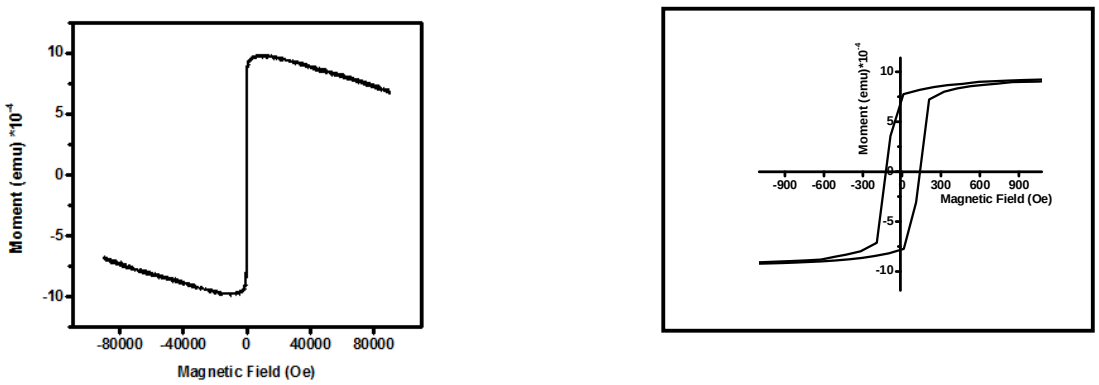

Figure 2.7: (a) Hysteresis loop of LSMO thin film (b) hysteresis loop at 4K (zoomed version of first image)

Magnetization versus temperature

The graph between the dependence of magnetization with temperature of LSMO thin film clearly shows a noticeable transition at 350K. Here there is a transition from ferromagnetic to paramagnetic phase. Ferromagnetic phase is highly ordered, as temperature increases randomisation starts and become paramagnetic.

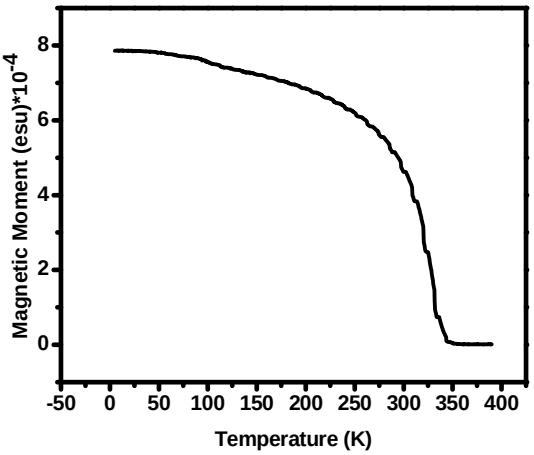

Figure 2.8: Temperature dependence of magnetization of LSMO thin film

Surface morphology

Surface morphology of LSMO films were analysed by investigating AFM images of surfaces in non-contact mode. The thickness of the film is 30 nm. We can see small grain sized particle which is distributed uniformly.

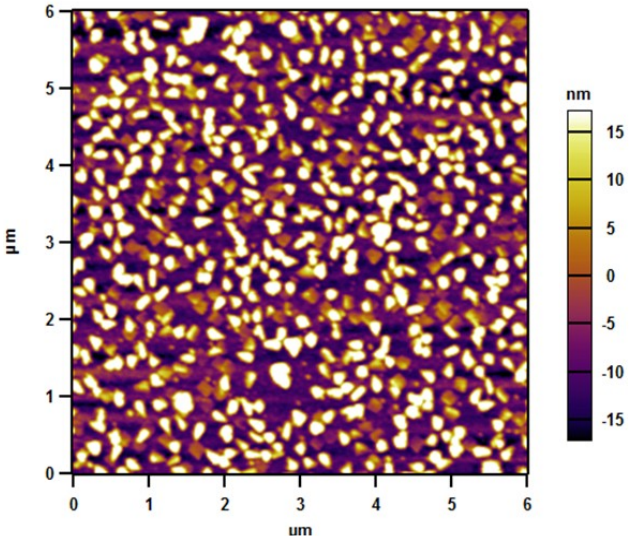

Figure 2.9: Topography of LSMO thin film of 6 × 6 μm^2

Scanning electron microscopy (SEM)

From the Figure 2.10, we get to know about the surface morphology of LSMO pellet. The energy of the electron beam used is 15keV. Particle roughness is in the order of 10 µm.

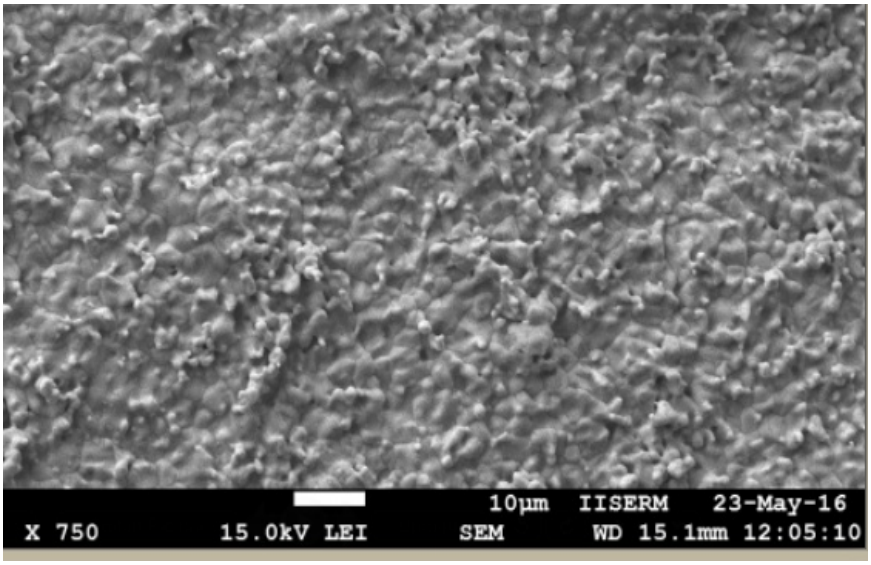

Figure 2.10: SEM image of LSMO pellet

Energy dispersive X-ray spectroscopy (EDAX)

The elemental confirmation of LSMO thin film and to get to know about the percentage of oxygen in the thin film.

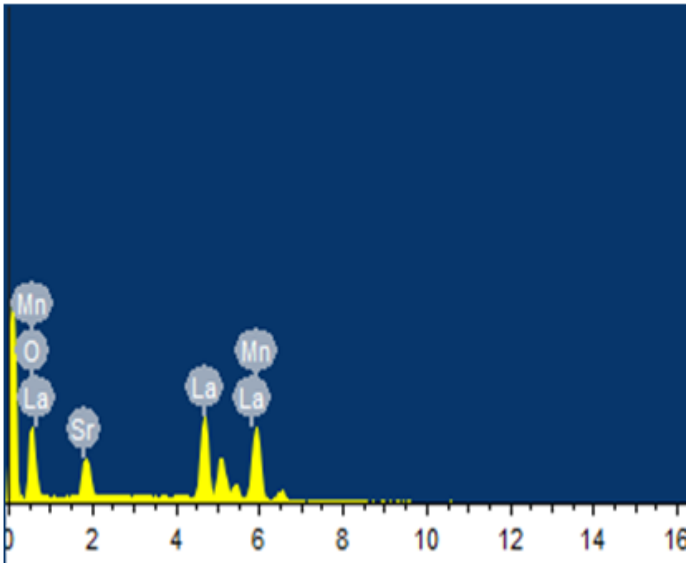

Element	Weight%	Atomic%
O K	24.86	65.26
Mn K	21.85	16.70
Sr L	10.89	5.22
La L	42.40	12.82

Figure 2.11: Elemental confirmation of LSMO thin film

2.2 Synthesis of Nickel

2.2.1 Preparation of Ni thin film

Thin film of Ni was prepared by dc magnetron sputtering in which our target is Ni and substrate is Si (100). For the preparation of the thin film first clean the substrate in sonicator and then mount the sample and target inside the chamber. Start the vacuum pumps and wait till the pressure inside the chamber is 10^{-6} mbar. When pressure is achieved then we started purging argon gas inside the chamber and flush out it for 2-3 times. After flushing out of argon gas now fill the chamber with argon gas for deposition. By adjusting the flow rate of argon gas, pressure of gas inside the chamber should be 0.13 mbar. Now set the substrate temperature at 300°C. After setting these parameters start the supply of dc voltage of 336 V and power is 0.101 kW. Thin film was prepared by varying the deposition time 30 minutes, 25 minutes and 20 minutes at same substrate temperature [9].

2.2.2 Characterization techniques:

We have measure the thickness of our thin film using AFM which is40 nm by masking the sample while sputtering as shown in Figure 2.12 and corresponding thickness profile shown in Figure 2.13

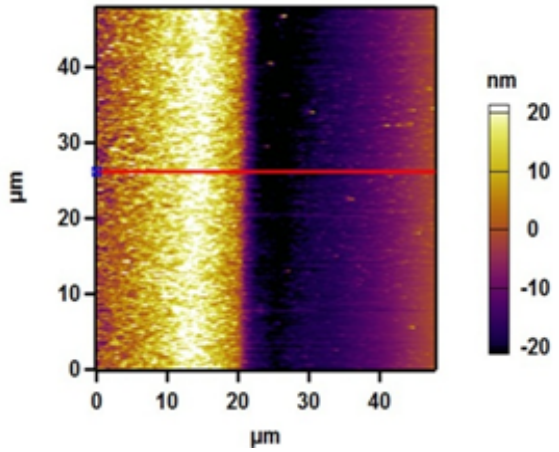

Figure 2.12: Topography of nickel thin film

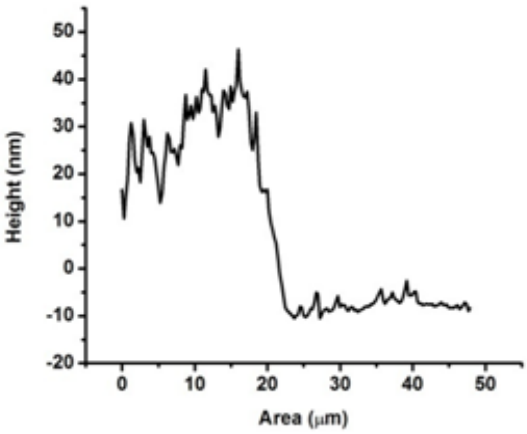

Figure 2.13: Thickness profile of Nickel thin film

MFM (Magnetic Force Microscopy) is one of the tools of AFM, where tip scans the magnetic sample and magnetic interaction between tip and sample is detected to reconstruct the structure of the sample surface. MFM scans in non-contact AFM mode. MFM is used to measure the domains of the film which can be further studied in the presence of varying external magnetic field and this measurement can be done at room temperature. The domain of Ni film is shown in
Figure 2.15.

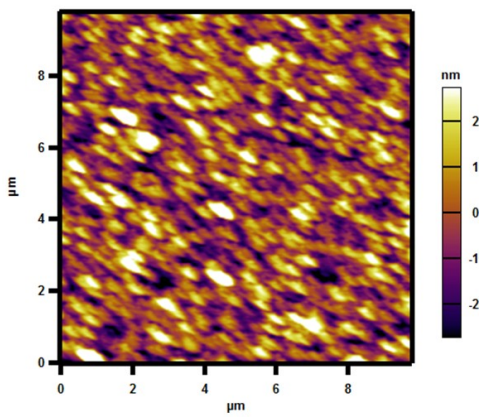

Figure 2.14: Topography of Ni/Si thin film

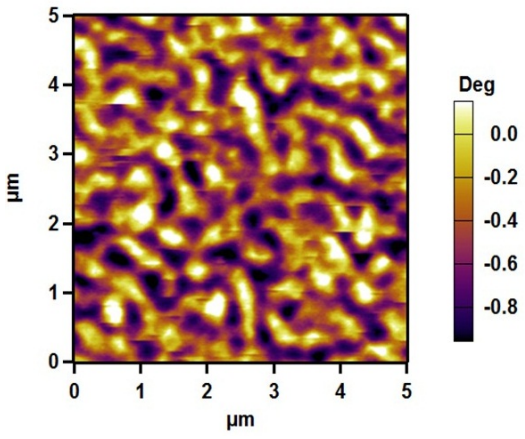

Figure 2.15: MFM image of Nickel thin film

Chapter 3

Synthesis of superconductor

3.1Brief history of superconductivity

The most unusual and interesting properties of solid is superconductivity in which its electrical resistance falls to zero where the solid is cooled to a suitably low temperature and specimen behave as perfect diamagnetic. The phenomenon of low temperature of superconductivity was first observed by Kamerlingh Onnes in 1911, Leiden. And the phenomenon of diamagnetism was discovered by Meissner and Ochsenfeld as a property of superconducting state in 1933. Then emerged Nobel theory of superconductivity in 1957, B.C.S theory predicted that critical temperature could never be higher than 30K. After observation of higher T_c in YBCO, people discovered Bismuth based and Thallium based superconductor with much higher T_c.

The characteristic signature of a superconductor

1. Zero resistance below critical temperature.
2. Negative susceptibility $\chi = -1$.
3. Perfect diamagnetism.

Superconductors are defined by three parameters

T_C – the highest temperature below which a material is superconductor.

H_c – above this value of external magnetic field, material will be non superconducting.

J_c – the maximum current that a superconductor can carry without any resistance.

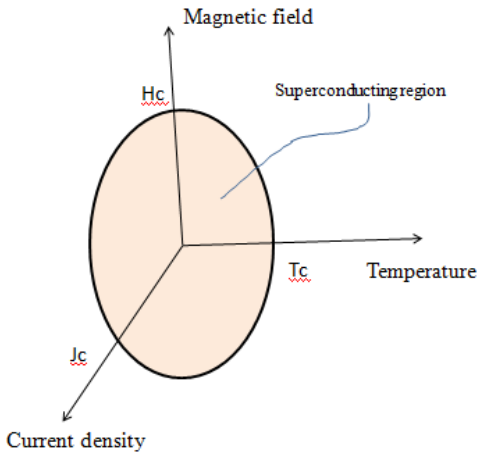

Figure 3.1: Superconducting surface with limit in T_C, J_C, and H_C.

Material will be non superconducting if it exceeds critical temperature, critical current and critical field. Superconducting surface is illustrated in the Figure 3.1

3.1.1 Superconductivity theory

BCS (Bardeen-Cooper-Schrieffer) in 1957 explain theory of superconductivity quite successfully. There is an existence of energy gap of Δ between superconducting state and normal one. Energy gap is due to binding of superconducting electron into cooper pairs. Which implies 2Δ is the energy required to break the cooper pair. This attractive interaction is due to lattice vibration. BCS theory starts with explaining about an attractive potential between electrons which can overcome columbic potential. An electron in a conductor is attracted by the positive potential by the lattice. This deformation of lattice cause an electron of opposite spin tends to move into higher positive charge density. The two electrons get correlated. So a pair of fermions is a boson and these pair condensate. These fermions pair is called as cooper pair.

3.1.2 Magnetic property of superconductors

Superconductors are classified as type 1 and type 2 depending on their behaviour towards magnetic field.

TypeI superconductor

Type I superconductors are the ones which follows strictly Meissner effect of perfect diamagnetism above the critical temperature. Beyond the critical temperature it will behave like normal conductors. They are known as soft superconductors.

Examples are all metals except Niobium

Type II superconductors

Type II superconductors violate the Meissner effect of perfect diamagnetism since it has two critical magnetic fields H_{c1} and H_{c2}. For H < Hc1 they behave as a perfect diamagnetism. In between H_{c1} and H_{c2} flux will penetrate. The region between H_{c1} and H_{c2} is called intermediate or vortex region. They have potential application in all field of life.

Examples are cuprates superconductors, Niobium

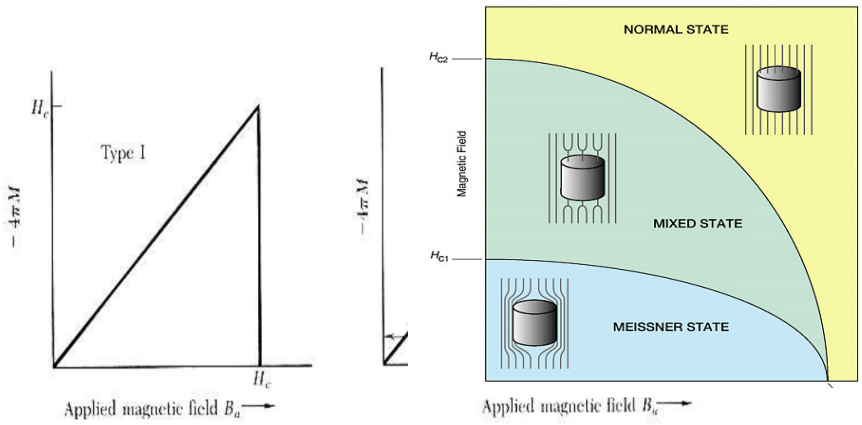

Type I superconductor

Type II superconductor

Figure 3.2: Magnetic behaviour of type I and type II superconductor

3.1.3 Characteristic property of superconductor

Meissner effect

Repulsion of magnetic field lines passing through the material above the critical magnetic field [10].

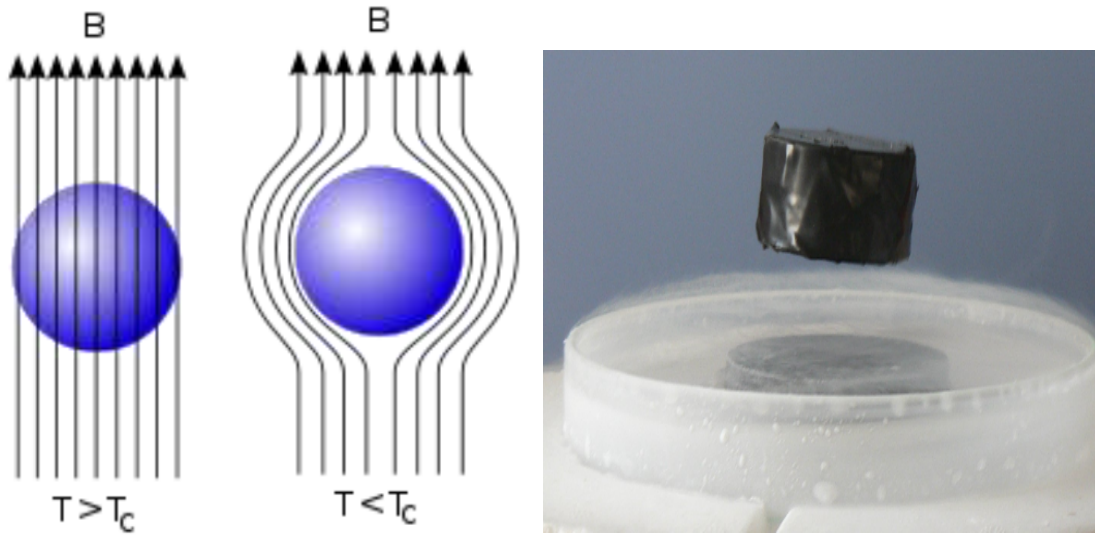

Figure 3.3: Meissner effect of superconductor (below the critical temperature).
(Source: https://www.quora.com/What-is-the-Meissner-effect)

Zero electrical resistance

When a material cool down below the critical temperature it will be superconductor, at that time it feels no electric resistance [10].

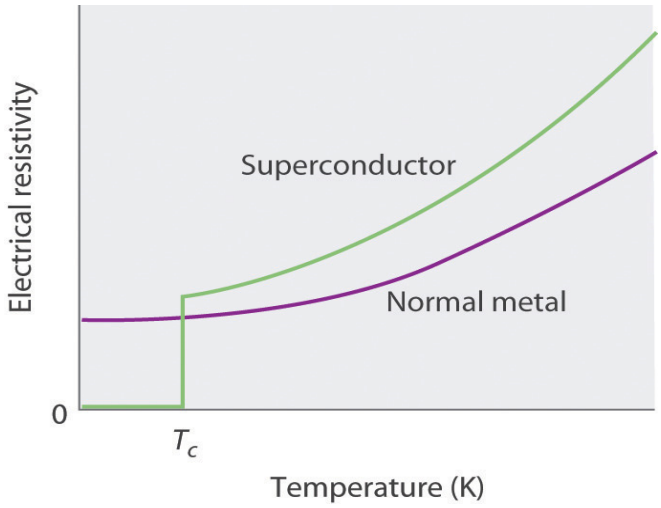

Figure 3.4: Zero resistance of superconductor.

(Source:https://ing.dk/artikel/ny-rekord-superledning-ved-203-kelvin-178033)

Specific heat

The specific heat of superconductor shows a transition at T_c since superconductor affects electron mainly so lattice vibration part remains unaffected and we find electronic specific heat is nonlinear with the temperature.

Magnetic field

The magnetic field induced inside the sample is given by

$$\boldsymbol{B} = \mu_0(\boldsymbol{H} + \boldsymbol{M})$$

Where $\boldsymbol{H}$ is external magnetic field and $\boldsymbol{M}$ is magnetization.

According to Meissner's law

$$\mu_0(\boldsymbol{H} + \boldsymbol{M}) = \boldsymbol{0}$$

That means $\boldsymbol{H} = -\boldsymbol{M}$

Which implies susceptibility is negative for superconductor [10].

3.2 High temperature superconductor Yttrium barium copper oxide (YBCO)

The orthorhombic crystal structure of YBCO is perovskite which has a general formula of ABO_3. In case of YBCO, A stand for Y or Ba and the system has deficiency of oxygen because of this it is known as oxygen deficient or distorted perovskite structure. The resulting metal oxygen layer can be illustrated as in the form of a sequence CuO – BaO – CuO_2 – Y – CuO_2 – BaO – CuO - The key feature of YBCO superconductor is its CuO_2 plane which is a square lattice formed connected each other via oxygen atoms. There is a possibility of copper atom to expand its co-ordination to four, five or six depending upon the each copper ion be co-ordinated to oxygen atom in the apex of an octahedron. The charge reservoir is CuO chain layer which supplies charge carrier to CuO_2 plane to induce superconductivity [11].

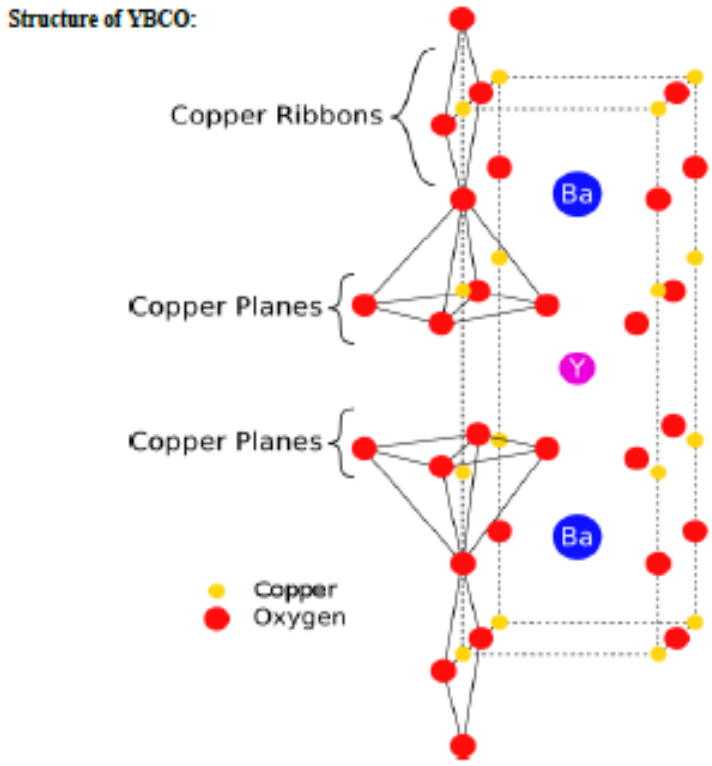

Figure 3.5: Structure of YBCO superconductor.

(Source: http://www.wikiwand.com/en/Yttrium_barium_copper_oxide)

3.2.1 Experimental section

Target preparation for pulsed laser deposition

Target preparation is the most important and the crucial step for thin film growth. Target plays a role in defining the stoichiometry, impurity content, surface morphology, etc. of the film. Typically target for PLD consist of a compacted pellet which has same stoichiometry of the desired film. Target preparation is usually by solid state reaction method.

High temperature superconductor target preparation can be summarised as follows

1. Assimilation the reagents
2. Calcinations with intermediary grinding
3. Annealing
4. Pressed into pellet

YBCO can be prepared by mixing the reagents as per balance equation

$$Y_2O_3 + 4BaCO_3 + 6CuO \rightarrow 2YBa_2Cu_3O_7 + 4CO_2$$

Steps involved in preparation

Yttrium oxide (Y_2O_3), Barium carbonate ($BaCO_3$), Copper oxide (CuO) are mixed in the ratio of 1: 2: 3. Precursor powder is grinded well by using mortar for 3-4 hours to get the uniformity and homogeneity of particle size. The grounded sample is transferred to alumina crucible and subjected to calcinations at 920°C for 24 hours for 3 times. Calcinated powder was pressed using hydraulic press. Finally YBCO pellet was sintered at 900°C for 12 hour and then annealed at 500°C for 2 hours in muffle furnace [11].

Laser parameter

To synthesise YBCO thin film by PLD process using excimer KrF laser of wavelength 248nm was directed onto the rotating YBCO target. Substrate was cleaned in sonicator for 20 minutes at 40 °C. Then mount the cleaned substrate with silver paste onto the heater. Place substrate at 8 cm from the target. The substrate temperature was measured by the sensor attached to it. When system reach the vacuum of 10^{-6} mbar m then laser fluence was maintained at 200 mJ with 5 Hz as repetition rate. Substrate temperature was

800°C. Total number of laser shots is 15,000.After deposition substrate temperature (STO 100) was cooled down to 550°C and annealed the system for 2 hours. The oxygen pressure was maintained at 0.4 mbar during deposition and was raised to 600 mbar slowly. The film was then slowly cooled down to room temperature [11].

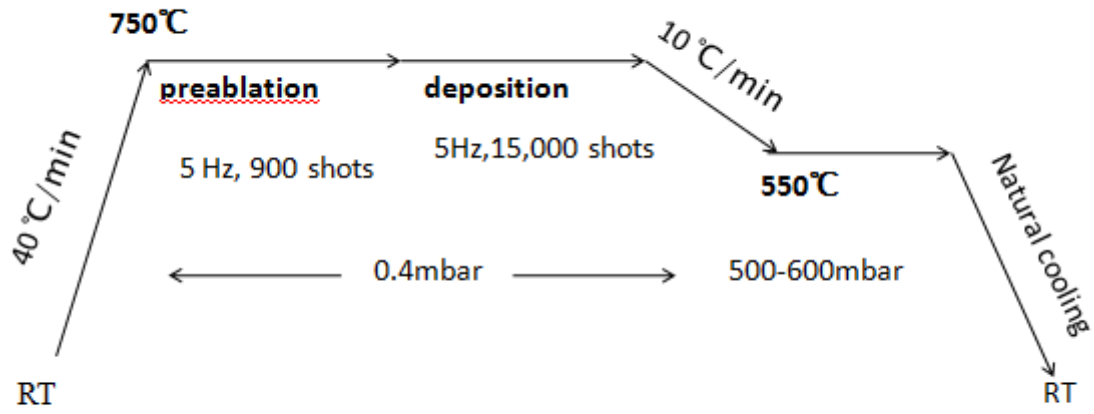

Figure 3.6: Schematic representation of YBCO thin film preparation

3.2.2 Characterisation Techniques

Structural characterisation of YBCO superconductor

We can measure critical temperature using R-T system. Critical temperature is an indicative of stoichiometry of the superconductor. By using four probe methods we can measure resistance – temperature dependence. We made four contacts on the surface of thin film using gold wire and silver paint. We kept the film in R-T probe and measure the voltage by passing milliampere current through the contacts. We measured the resistance (Ohm's law) of thin film against temperature ranging from 2K to 180K.

R-T measurement

From the Figure 3.7 (a) we are getting a transition of 90K for YBCO thin film of thickness 40 nm. Transition is sharp but resistance is not exactly zero. It may be due to defects in film.

From the Figure 3.7 (b) we can infer that transition is at 95K and transition is broad for YBCO pellet. Below the transition temperature resistance is becoming zero. Transition temperature is higher for bulk sample when compared to thin film.

(a) (b)

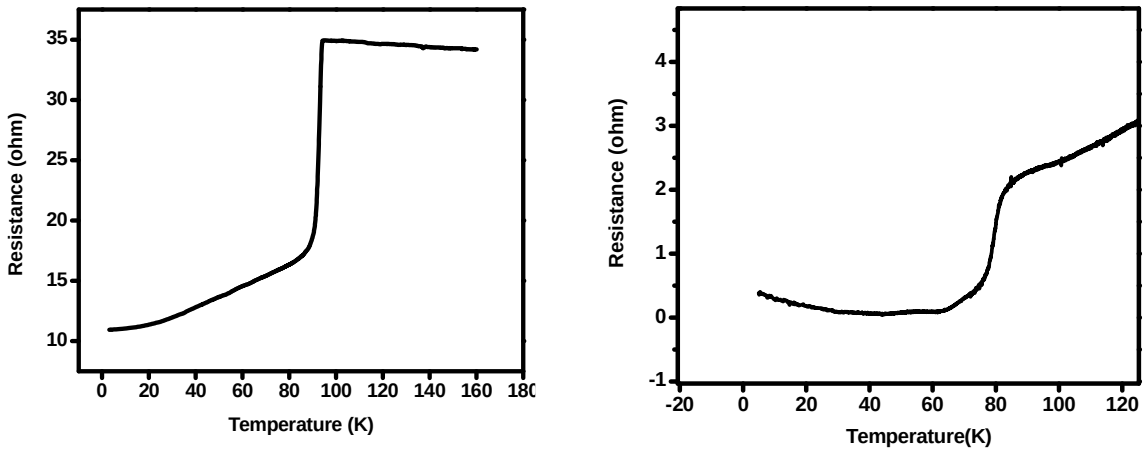

Figure 3.7 (a): Resistance temperature graph of YBCO thin film. Figure 3.7(b): Resistance temperature graph of YBCO pellet

Topography of thin film

Topography of YBCO thin film is shown in the Figure 3.8. Particle size is approximately 40nm.

(a) (b)

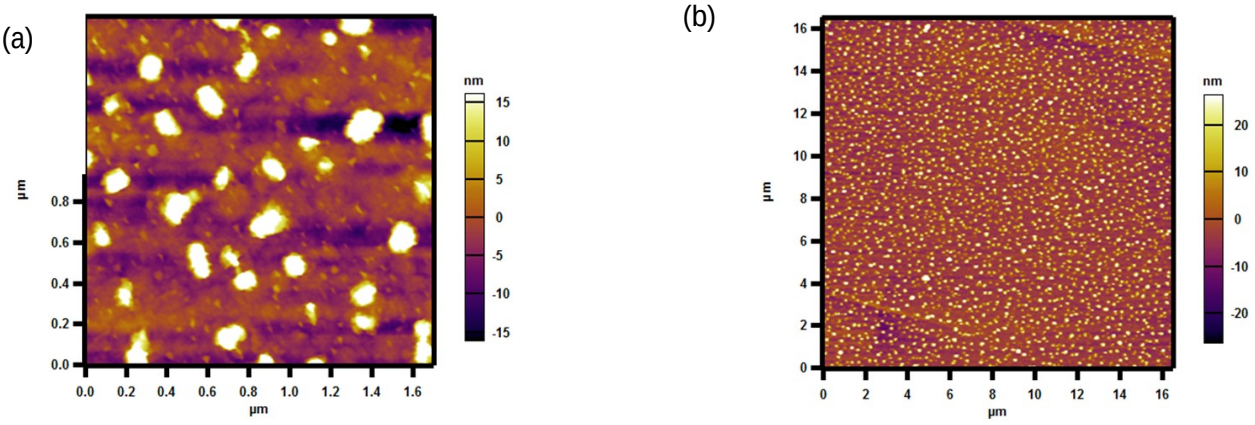

Figure 3.8: (a) Non contact topographic image of YBCO thin film 1.7 × 1.7 μm^2.(b) Non contact topographic image of YBCO thin film 17 × 17 μm^2

X-ray crystallography

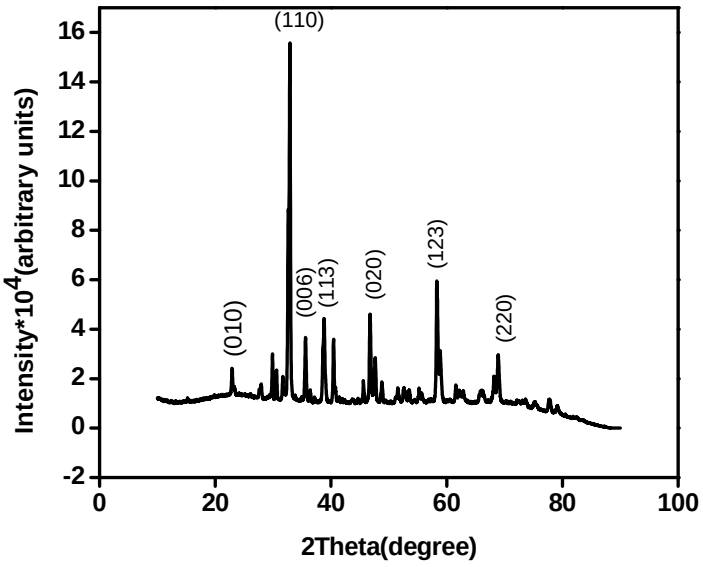

Figure 3.9: XRD of YBCO superconductor (in powder form)

Figure 3.9 shows the XRD pattern of YBCO thin film of thickness 40nm. Indexing of pattern shows that all samples are in orthorhombic structure P_{mmm}. From the XRD data we can confirm that the stoichiometry of YBCO is 1: 2: 3: 6.9. Analysis of XRD data reveals that oxygen content is controlled by the oxygen pressure during the deposition. By controlling the oxygen pressure we will get the YBCO in single phase.

3.3 Synthesis of Bismuth strontium calcium copper oxide (BSCCO)

$$Bi_2O_3 + SrCO_3 + CuO + CaCO_3 \rightarrow Bi_2Sr_2CaCuO_6 + CO_2$$

To prepare pellet of superconducting BSCCO, first we have to prepare BSCCO powder starting from precursor powders. Solid state synthesis method is most frequently used for the preparation of BSCCO. This method involves the mixing of oxides and carbonates of Bismuth, Strontium, Copper and Calcium. The powders of Bi_2O_3, $SrCO_3$, CuO and $CaCO_3$ are weighed accurately and grind it in agate mortar and pestle. During heat treatment intermediate grindings are necessary for uniformity and to make desirable the particle size. Calcinations are used to achieve the desired crystal phase and particle size. For the heating of material high melting point container is used i.e. alumina crucibles (Al_2O_3). Then the mixture is calcinated in three stages and make pellet out of it finally we

sintered pellet .The heating rate of furnace is 5°C /min and intermediate grinding is done at the end of each heating cycle [12].

3.3.1Thin film preparation

First take STO substrate, clean it in a sonicator using isopropyl alcohol at 40^0C for 20 minutes and dry it with nitrogen gas. Now mount the sample and target inside the chamber. To generate vacuum, switch on the rouging pump and then turbo molecular pump. When pressure inside the chamber reach to 10^{-5} or 10^{-6} mbar, start inserting oxygen gas inside the chamber (for the preparation of oxides film oxygen is used as background gas). Now flush out oxygen gas for two to three times and then set temperature parameters i.e. deposition was done at temperature 800^0C and the pressure of oxygen inside the chamber while deposition is 2mbar. The film was annealed at 780^0C for about 4h and cool down at room temperature for about 76 minutes (10^0C/min). The pressure of oxygen while annealing is also 2mbar [12].

The target was ablated for 10 minutes before deposition and the excimer laser (λ = 248nm) was operated at 229mJ/pulse for 45-50 minutes.

3.3.2 Characterisation techniques

AFM Image

Surface topography of the film indicate that the particle size is of the order of 300nm

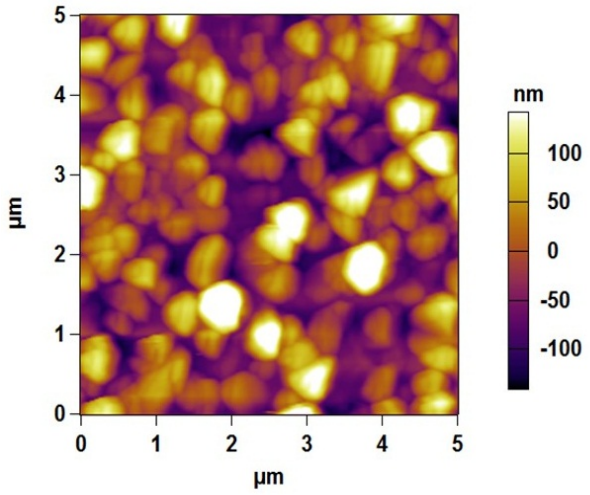

Figure 3.10: Topography of BSSCO thin film 5 × 5 μm^2

X- ray crystallography

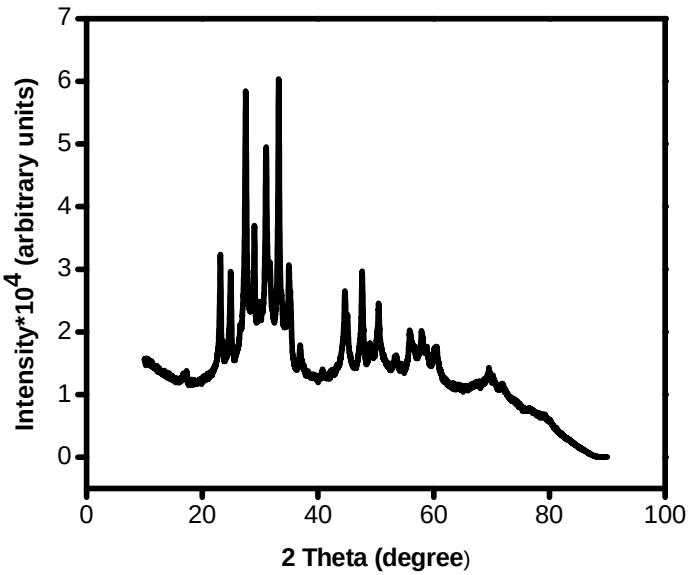

Figure 3.11: XRD of BSCCO thin film

Resistance-temperature graph

BSCCO thin film is having two transitions one is at 100K and another is at 80K. Actual transition temperature of BSCCO is 90K. Which means there exist two phases of BSCCO in which one is superconducting in nature.

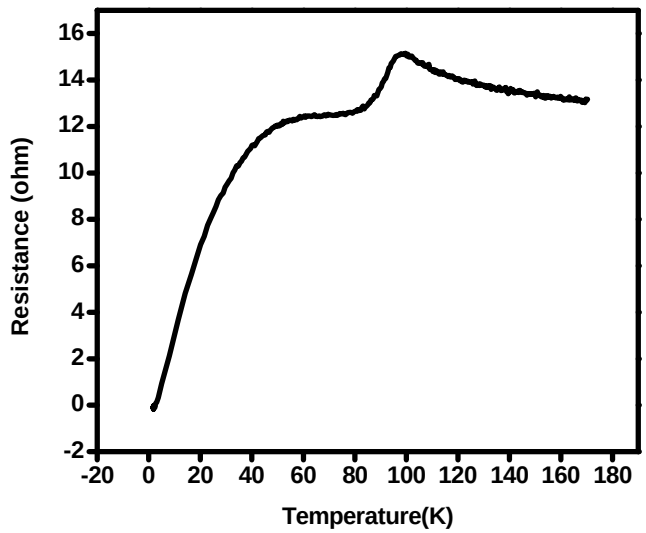

Figure 3.12: R-T of BSCCO thin film

3.4 Synthesis of Niobium thin film

Niobium is the only metal which behaves as type 2 superconductor. It has potential application in RF field cavities and Josephson junction in superconducting electronics. We are aiming to grow niobium film with T_c greater than 8K.

3.4.1 Thin film preparation

Nb film was grown over silicon substrates (100). For deposition using sputtering we are using target from Kurt – Lesker (99. 9%).The base pressure was in the range of 10^{-6}mbar. Niobium thin film was grown over different substrate temperature and different power by keeping the pressure constant. We optimised the best suited condition for the growth of the thin film.

We cleaned the substrate in propyl alcohol by ultrasonication and paste in substrate holder using silver paint. Niobium thin films were prepared by dc sputtering in high vacuum system of 10^{-6} mbar. Once high vacuum is achieved, heat the substrate to 800°C. Purge the system with argon gas and flush the system. For deposition keep Argon pressure at 1.4×10^{-1}mbar. The power of sputtering is 0.130W and the deposition time is 20 minutes. Repeat the experiment by varying power and substrate temperature [13] [14].

3.4.2 Characterisation techniques

When we keep the substrate temperature at 800℃ and power is 130W. We are getting a sharp transition at 2K as shown in the Figure 3.13. But actually, transition temperature of niobium is at 9K. When we increase the power to 200W we are getting a transition at 3.5K as in Figure 3.14. Finally, when the power becomes 220W we are getting a sharp transition at 6.5K as in Figure 3.15.

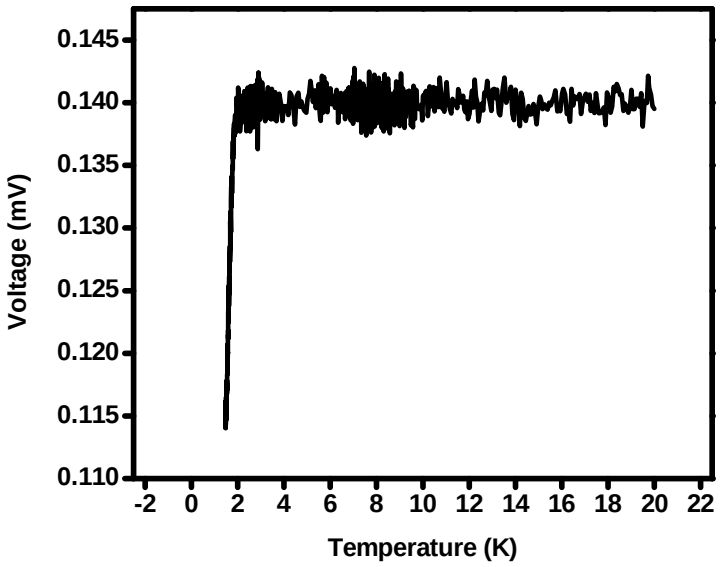

Figure 3.13: Niobium thin film prepared at substrate temperature of 800°C and power 130W.

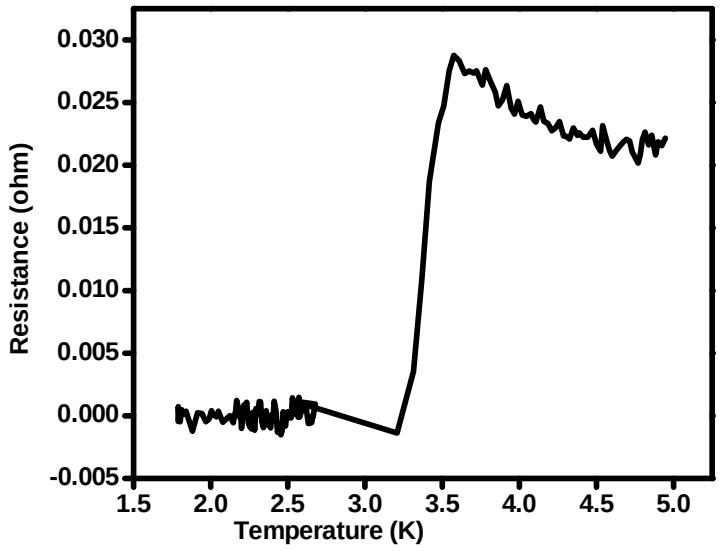

Figure 3.14: Nb film is grown at a substrate temperature of 800°C and Power 200W.

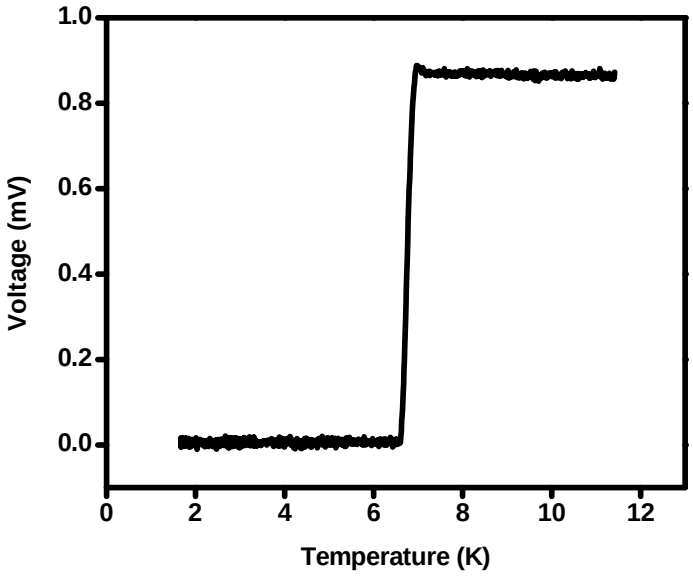

Figure 3.15: Nb thin film grown over silicon substrate at power of 220W

Topography

Topography of Nb thin film over silicon (100) is shown in Figure 3.16(a) Particle size is approximately 20nm which is grown at a substrate temperature of 700℃. Figure (b) Nb film grown over silicon substrate at a temperature of 600℃having a particle size of 6nm.

(a) (b)

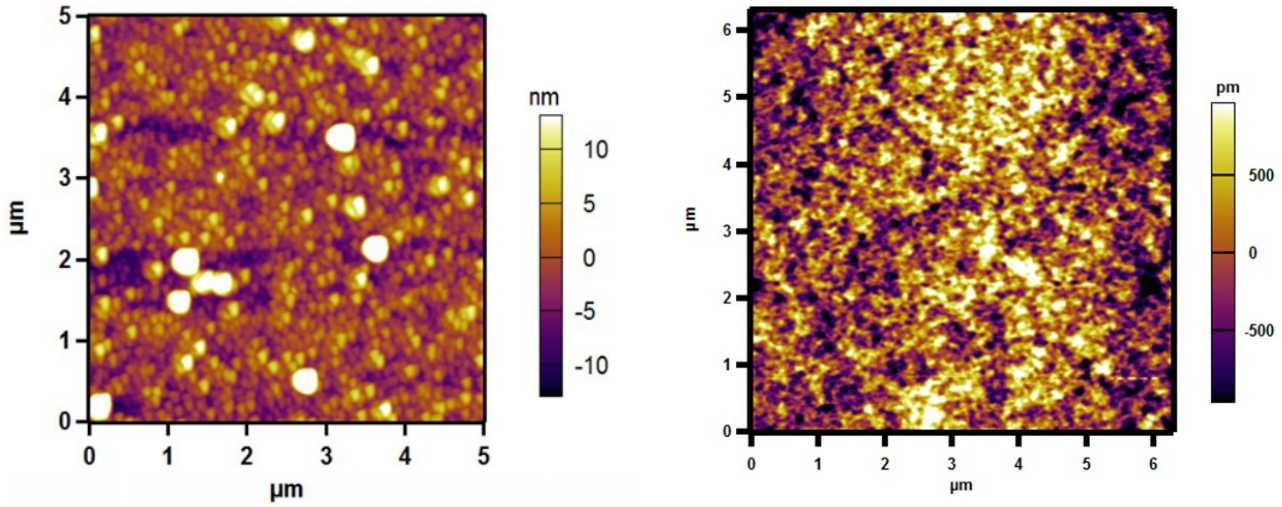

Figure 3.16: Topography of Nb/Si (a) substrate temperature of 700℃, (b) substrate temperature of 600℃.

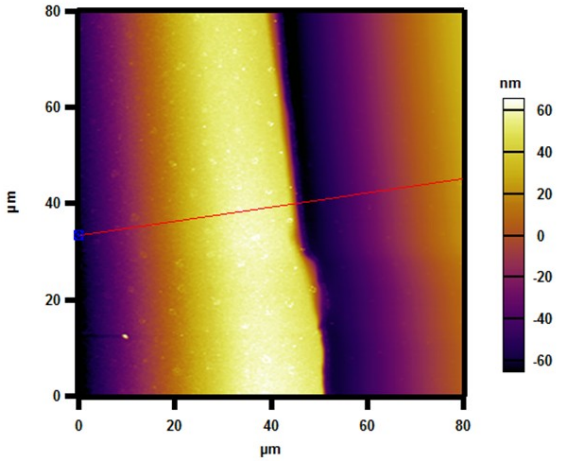

Figure 3.16(c): Masked sample of Nb/Si

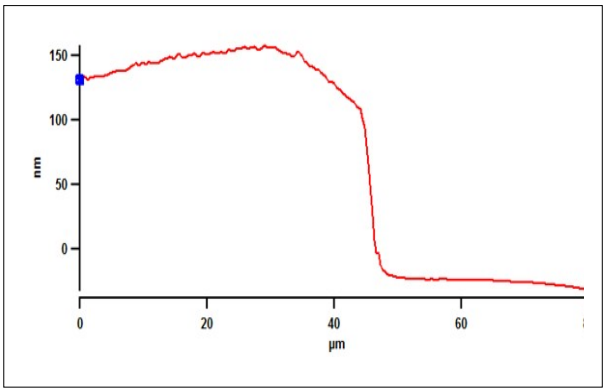

Figure 3.15(d): Particle height distribution in Nb/Si

EDAX analysis

EDAX will give a measure of amount of oxygen that is present in Niobium thin film. Since Niobium is highly susceptible to oxidation.

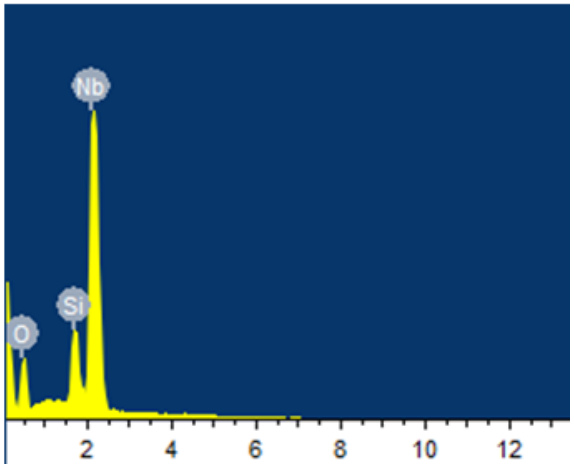

Element	Weight%	Atomic%
O K	17.47	51.28
Si K	5.99	10.02
Nb L	76.54	38.70
Totals	100.00	

Figure 3.17: Shows the elemental analysis of Niobium thin film

3.5 Synthesis of Niobium Nitride thin film

3.5.1 Synthesis, optimisation of niobium nitride thin films

NbN films are synthesised by on Si (100), MgO (100) and $SrTiO_3$ (100) substrates. We optimise growth condition by adjusting the sputtering power and the ratio of Ar:N_2 mixture.

Optimised condition

The substrates (MgO, SrTiO3) were placed on substrate holder. When the pressure of the chamber become 10^{-6} mbar, at this point substrate heater was turned on and substrate was heated to 800 °C. Flushed the system with argon and nitrogen gas two or three times to make sure that system is free from foreign molecules. First argon was flushed into the chamber at the rate of 26.5 sccm to adjust system pressure at 3.9×10^{-2} mbar. After three minutes of deposition nitrogen gets introduced into the system at the rate of 8 sccm. When deposition is about to started make pressure to 3.3×10^{-3}mbar. Remove the mask from the target and start the reactive sputtering and keep it for 10 minutes. Once the deposition is over keep it in base pressure until the system cool down [15],16].

3.5.2 Characterisation techniques

XRD data

There is a peak at 41^0 corresponds to NbN (200). Nb_2N peak is at (101). MgO peak is at (200) 58^0. From XRD it is confirmed that Niobium Nitride has been formed.

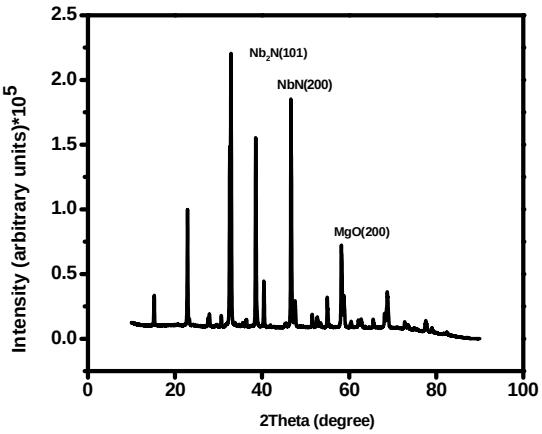

Figure 3.18: XRD of NbN/MgO data

SQUID Measurement

From the Figure we can see that transition temperature of Nb/Si is 12K and transition temperature of Nb/STO is 10.5K.

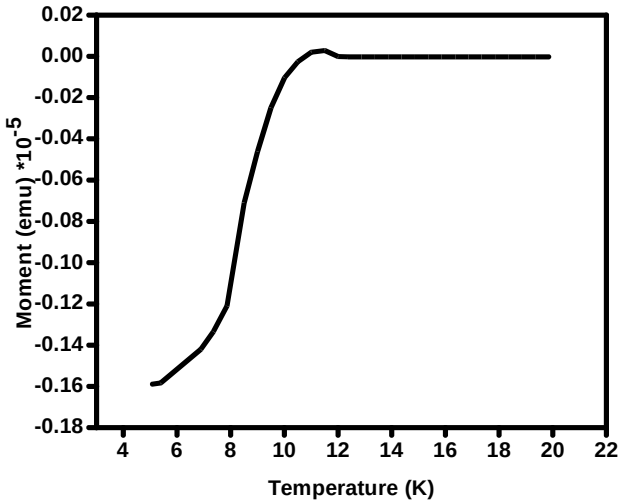

Figure 3.19(a): Moment v/s Temperature Nb/Si

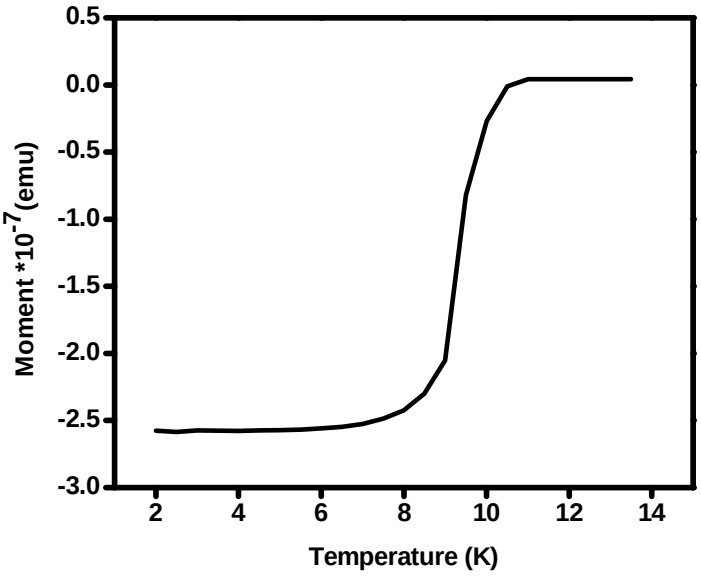

Figure 3.19(b): Magnetic moment versus Temperature graph of Nb/STO

EDAX

From EDAX it is confirmed that thin film is of Niobium Nitride.Thin film of NbN contains low content of oxygen.

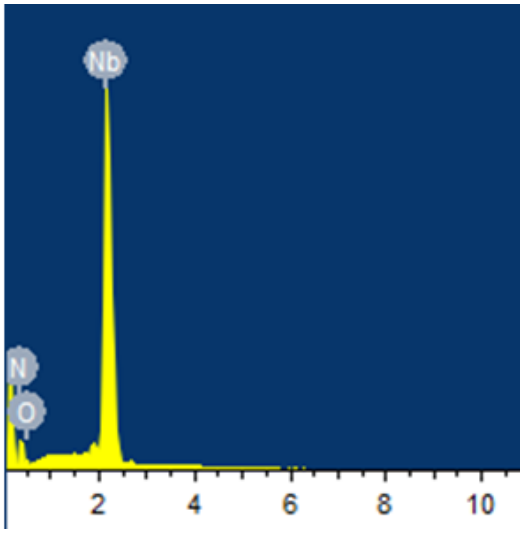

Element	Weight%	Atomic%
N K	16.24	54.06
O K	1.62	4.72
Nb L	82.14	41.22
Totals	100.00	

Figure 3.20: EDAX of NbN by eliminating substrate peak MgO.

Surface Topography

From the topography we can conclude that NbN/STO thin film has a particle size of 1.5nm, which indicate that thin film is smooth.

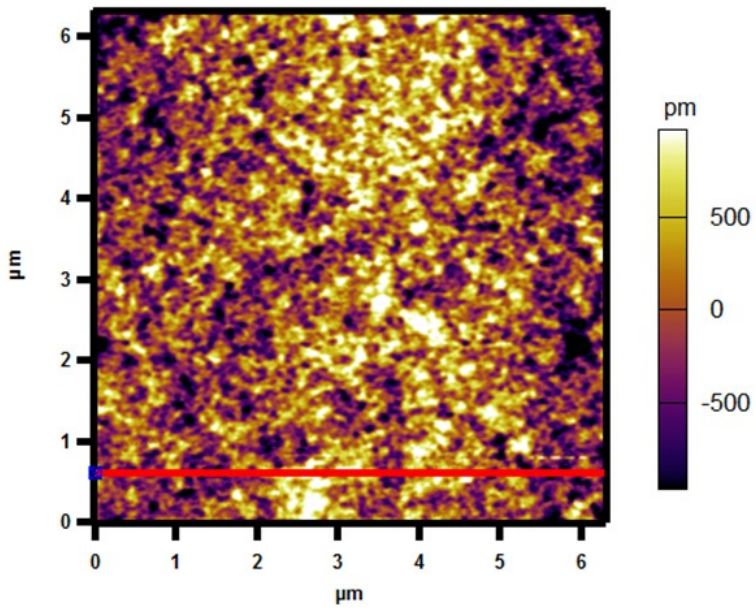

Figure 3.21: Topography of NbN/STO

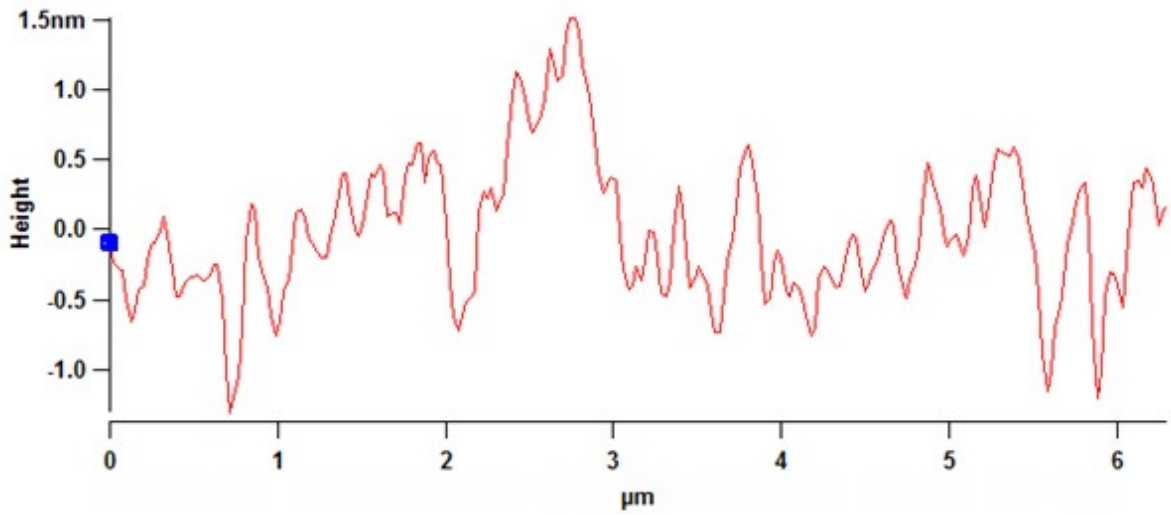

Figure 3.22: Particle size distribution in NbN/STO

3.6 Synthesis of Tantalum nitride

TaN films are synthesised by depositing on substrate such as MgO (100) and $SrTiO_3$ (100). Tantalum target will react with the mixture of argon and nitrogen in a particular ratio to undergo reactive DC sputtering. We optimised growth condition by adjusting the sputtering power and the ratio of Ar: N_2 mixture.

3.7.1 Thin film preparation optimised condition

The substrates (MgO, SrTiO3) were placed on substrate holder at a distance of 8cm from the target. When the pressure of the chamber becomes 10^{-6}mbar, at this point substrate heater was turned on and substrate was heated to 800 ℃.

Flushed the system with argon and nitrogen gas two or three times to make sure that chamber is free from foreign molecules. Argon was flushed into the chamber at the rate of 30 sccm and the system pressure was at 3.9×10^{-2}mbar. After three minutes of preablation nitrogen gets introduced into the chamber at the rate of 8 sccm. When deposition is started adjust the pressure to 3.3×10^{-3}mbar. Remove the mask from the target and start the reactive sputtering and for 10 minutes. Once the deposition is over keep the system in base pressure until the system cools down [18], [19], [20].

3.7.2 Susceptibility graph

From the figure 3.23 there is a transition is at 6.5 K. Transition is sharp but still thin film is having some resistance.

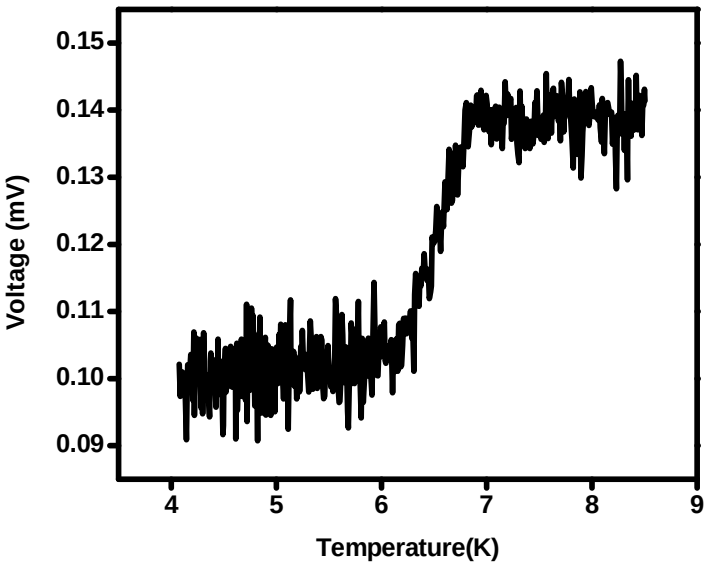

Figure3.23: Susceptibility of TaN thin film

Chapter 4

Synthesis of Ferrimagnetic insulator Yttrium Iron Garnet (YIG)

4.1Optimised condition for YIG thin film

Yttrium iron garnet ($Y_3Fe_5O_{12}$) thin films are prepared by pulsed laser deposition using a KrF excimer laser with base pressure of 10^{-6} mbar. The laser was focussed to energy of 191 mJ with a frequency of 6 Hz and 8000 shots. The material vaporised from the target was deposited onto the substrate quartz (100). Film was grown at the substrate temperature of 800 °C. The background gas was oxygen at the pressure of 1.33×10^{-1} mbar. Film was annealed after deposition for 10 minutes at 800 °C and the cool back to room temperature [21].

X-ray crystallography

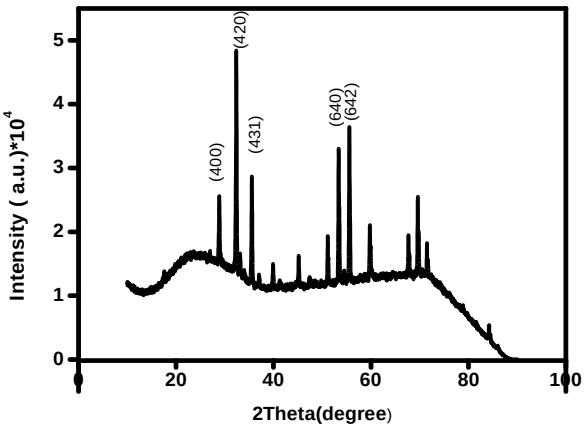

Figure4.1: XRD of YIG thin film on quartz

Surface Morphology

We looked at the topography of the YIG thin film and find out that the size of particle in the order of 6nm as shown in the Figure 4.2. Being ferromagnetic in nature there were magnetic domains were present as in Figure 4.3.

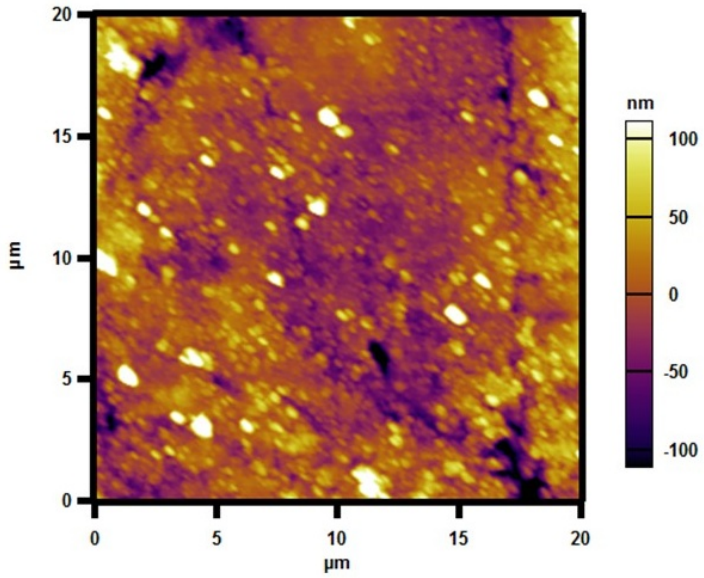

Figure 4.2: Topography of YIG thin film 50 × 50 µm^{2}in noncontact mode.

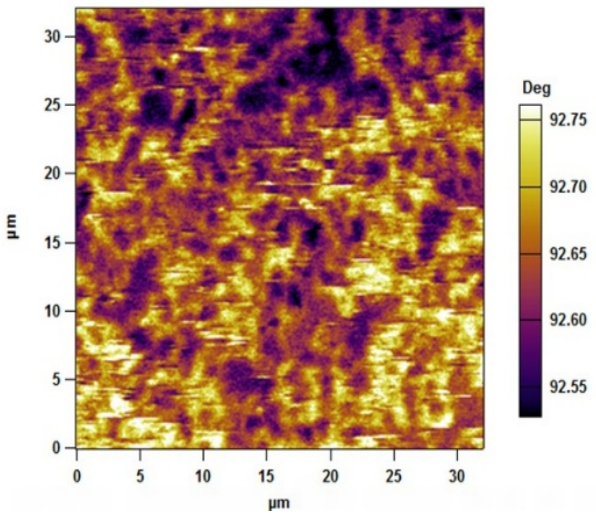

Figure 4.3: MFM image of YIG thin film 35 × 35 µm^2.

Chapter 5

Fabrication and characterisation of superconductor-ferromagnetic heterostructure

5.1 Proximity effect in superconductor/ferromagnetic heterostructure

Contact of material with different long range ordering modifies their properties near interface [22]. If we consider superconductor – metal interface, cooper pair can penetrate through normal metal to its thermal diffusive length. Superconducting properties are induced on normal metal and this phenomenon is called proximity effect. Due to the leakage of cooper pair to the metal surface leads to weakening of superconductivity of superconductor at the interface which is named as inverse proximity effect. As a result of inverse proximity effect there is a shift in the transition temperature of superconductor which is in contact with normal metal [23]. This entire phenomenon based on proximity effect reviewed by Deutscher and de Gennes on 1969.

Due to proximity effect superconductivity can be induced on the superconductor/ferromagnetic interface. There is a unique possibility to study electron pair in such a huge magnetic field. So, it opens a possibility of interplay of magnetism and superconductivity at nanoscale thickness range. Thus, we have two competing ordering in a controlled manner. On 1964, Larkin, Ovchinnikov, Fulde, Ferrel showed that there exists a ferromagnetic superconductor where its superconductivity is not uniform at low temperatures.

We are looking at the magnetic vortices induced in a ferromagnetic/ superconductor heterostructure. Superconductors that are used for this purpose are type 2 superconductors which have magnetic vortices. Our aim is to prepare thin film like the Figure 5.1 and magnetic pinning is shown in Figure 5.2

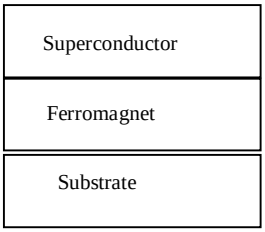

Figure 5.1: Superconductor/ferromagnetic heterostructure thin film

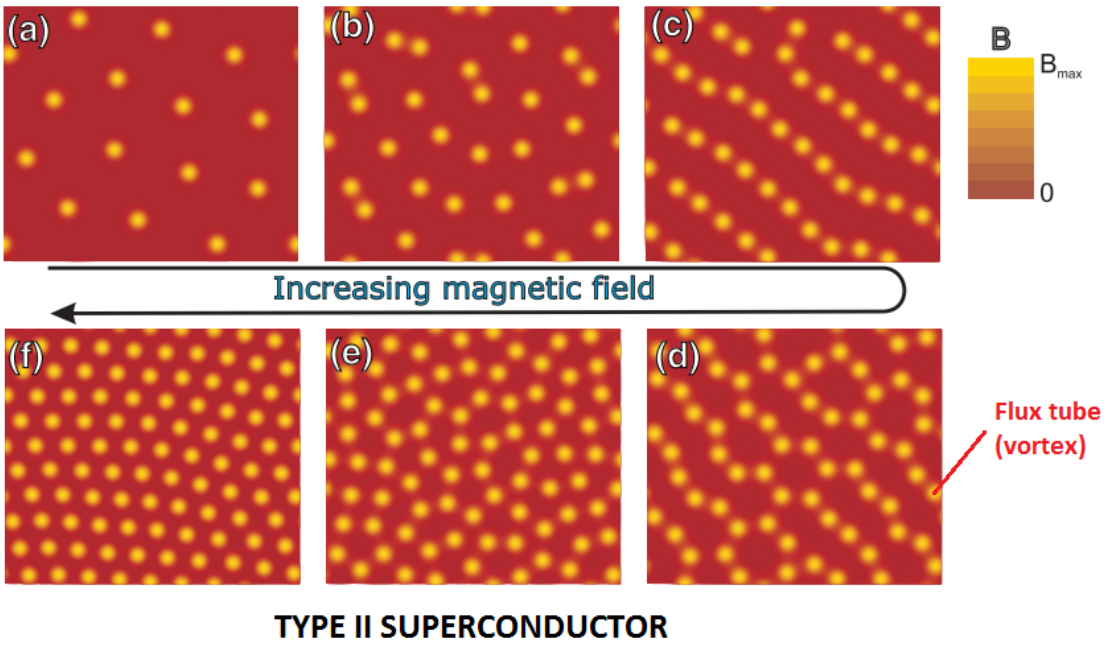

Figure 5.2: Magnetic vortices in type 2 superconductor as we increase magnetic field.

(Source:http://web.mit.edu/8.334/www/grades/projects/projects14/TrungPhan_8334WP/foundation-5.2.2/I_3.html)

5.2 LSMO/YBCO Heterostructure

Pulsed laser depositions were used to grow F (Ferromagnetic LSMO) and S (superconductor YBCO) structures. The polycrystalline LSMO were directly deposited on to the surface of STO (PLD optimised parameter). Thickness of LSMO was about 30nm. Without breaking the vacuum start depositing YBCO (using optimised parameter) of desired thickness of 40nm. The bilayer thin film was annealed at 550 °C.

AFM image

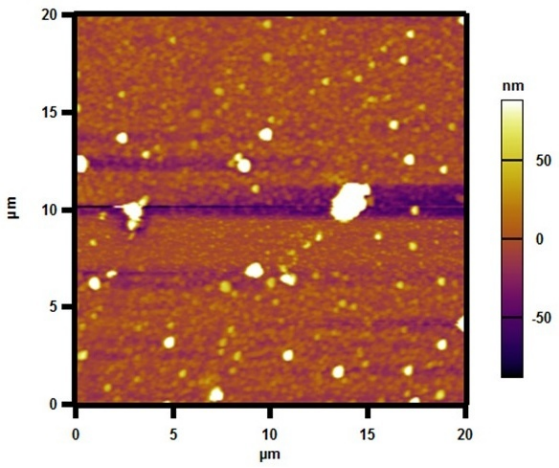

Figure 5.3: Topographic image of LSMO/YBCO bilayer, with a particle size of 20nm.

Vibrating sample magnetometer

Hysteresis loop is small when compared with LSMO thin film but still it is showing hysteresis.

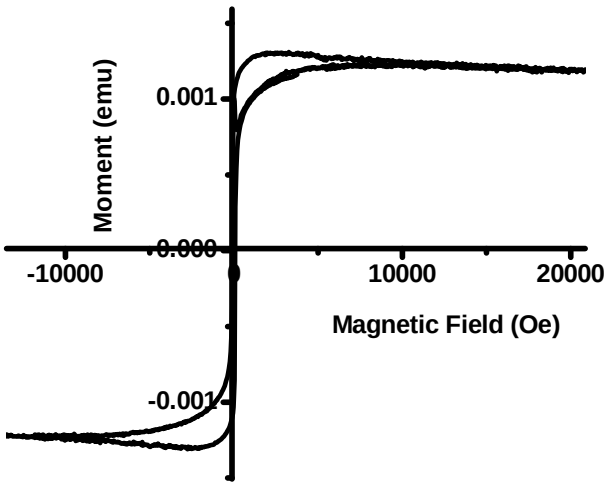

Figure 5.4: Hysteresis loop at 4K of LSMO/YBCO bilayer.

5.2 Conclusion and Future work

We prepared various thin films of superconductor, ferromagnetic and ferrimagnetic materials. We optimised the condition and successfully characterized the same using various techniques. By using multilayer films, we want to investigate magnetic vortices.

Bibliography

[1] H M Christen and G Eres.et.al. Recent advances in pulsed-laser deposition of complex oxides, J. Phys.: Condens. Matter,**20**, 264005, (2008).

[2] T. Venkatesan.et.al. Observation of two distinct components during pulsed laser deposition of high Tc superconducting films, Appl. Phys. Lett.**52**, (1988).

[3] P.J. Kelly, R.D. Arnell.et.al. Magnetron sputtering: a review of recent developments and applications, Vacuum, **56**, 159-172, (2000).

[4] G.Binning,C.F Quate, C.Gerber, Atomic Force Microscopy, Phys.Rev.Lett.**56**,930-934(1998)

[5] Franz.J.Giessibl, Advances in atomic force microscopy, Review of modern physics,**75**,949-983, (2003)

[6] Milton Ohring, The material science of thin film

[7] A. K. Debnath and J. G. Lin, Superconducting and transport properties of $YBa_2Cu_3O_7$ /La0.7Sr0.3MnO_3 bilayers Phys. Rev. B. **67**, 064412, 2003.

[8] Khalid Sultan, M. Ikram, Sanjeev Gautam.et. al. Electrical and magnetic properties of the pulsed laser deposited Ca doped LaMnO3 thin films on Si (100) and their electronic structures,**5**, 69075, (2015).

[9] Kazuki Yoshimura.et.al. Nickel Oxide Electrochromic Thin Films Prepared by Reactive DC Magnetron Sputtering, Japanese Journal of Applied Physics, **34**, Part 1, 5A.

[10] Charles Kittel, 'Introduction to solid state physics', **7th** edition, 335-361

[11] M. K. Wu, J. R. Ashburn, C. J. Torng, P. H. Hor, R. L. Meng, L. Gao, Z. J. Huang, Y. Q. Wang, Phys. Rev. Lett.**58**, 908-910, (1987).

[12] M Viret, J F Lawler and J G Lunney, Synthesis of BiSrCaCuO thin films by in situ and ex situ pulsed laser deposition, Supercond. Sci. Technol.**6**,490-496 (1993).

[13] Robert B. Bass, Lydia T.Lichtenberger and Arthur W. Lichtenberger, Effects of Substrate Preparation on the Stress of Nb Thin Films.

[14] Volha A. Matylitskaya, 1, Oliver Brunkahl1 , Gerald Kothleitner, Wolfgang Bock , and Bernd O. Kolbesen, Annealing of evaporated and sputtered niobium films in oxygen and nitrogen rich atmospheres by Rapid Thermal Processing (RTP), phys. stat. sol. (c), **4**, No. 6, 1802–1816 (2007).

[15] M. J. Deen, The effect of the deposition rate on the properties of d.c.-magnetron-sputtered niobium nitride thin films, Thin Solid Films, **152,** 535-544, (1987)

[16] S.K. Kim, B.C. Cha, J.S. Yoo, Deposition of NbN thin films by DC magnetron sputtering process, Surface and Coatings Technology 177 – 178, 434–440, (2004).

[17] E. J.Cukauskas, W. L.Carter and S. Qadri, Superconducting and structure properties of niobium nitride prepared by rf magnetron sputtering, J. Appl. Phys. **57**, **7**, (1985).

[18]H.B. Niel, S.Y. Xu1, S.J. Wang.et.al. Structural and electrical properties of tantalum nitride thin films fabricated by using reactive radio-frequency magnetron sputtering, Appl. Phys. A, **73**, 229–236 (2001)

[19] T. Elangovana, S. Murugeshan.et.al. Synthesis and high temperature XRD studies of tantalum nitride thin films prepared by reactive pulsed dc magnetron sputtering, Journal of Alloys and Compounds, **509**, 6400–6407, (2011).

[20] Xin Sun, Elzbieta Kolawa.et.al, Properties of reactively sputter-deposited Ta-N thin films, Thin Solid Films, **236,** 347-351, (1993).

[21] Y. Dumont, N. Keller.et.al. modified magnetic properties of oxygen off yttrium iron garnet thin film, Journal of Magnetism and Magnetic Materials **272**, E869 (2004).

[22] A. I. Buzdin. Proximity effects in superconductor-ferromagnet heterostructures. Rev of Mod Phy.**77,** (2005).

[23] M D Lawrence. et. al. Proximity effects in superconductor–ferromagnet junctions. J. Phys.: Condens. Mater.**11,**1089–1094, (1999).